

Manuscript version: Author's Accepted Manuscript

The version presented in WRAP is the author's accepted manuscript and may differ from the published version or Version of Record.

Persistent WRAP URL:

<http://wrap.warwick.ac.uk/161349>

How to cite:

Please refer to published version for the most recent bibliographic citation information. If a published version is known of, the repository item page linked to above, will contain details on accessing it.

Copyright and reuse:

The Warwick Research Archive Portal (WRAP) makes this work by researchers of the University of Warwick available open access under the following conditions.

Copyright © and all moral rights to the version of the paper presented here belong to the individual author(s) and/or other copyright owners. To the extent reasonable and practicable the material made available in WRAP has been checked for eligibility before being made available.

Copies of full items can be used for personal research or study, educational, or not-for-profit purposes without prior permission or charge. Provided that the authors, title and full bibliographic details are credited, a hyperlink and/or URL is given for the original metadata page and the content is not changed in any way.

Publisher's statement:

Please refer to the repository item page, publisher's statement section, for further information.

For more information, please contact the WRAP Team at: wrap@warwick.ac.uk.

JBR 21-117.R1

Cell-type specific circadian bioluminescence rhythms in *Dbp* reporter mice

Short Running Title: Bioluminescence Rhythms in *Dbp* reporter mice

^{a,b,1,2}Ciearra B. Smith, ^{a,c,1}Vincent van der Vinne, ^dEleanor McCartney, ^eAdam C. Stowie, ^fTanya L. Leise, ^{d,3}Blanca Martin-Burgos, ^dPenny C. Molyneux, ^gLauren A. Garbutt, ^hMichael H. Brodsky, ^eAlec J. Davidson, ^dMary E. Harrington, ^gRobert Dallmann, and ^{a,b,i,4}David R. Weaver

^a Department of Neurobiology, University of Massachusetts Chan Medical School, Worcester MA

^b Graduate Program in Neuroscience, University of Massachusetts Chan Medical School, Worcester MA

^c Department of Biology, Williams College, Williamstown, MA

^d Neuroscience Program, Smith College, Northampton MA

^e Neuroscience Institute, Morehouse School of Medicine, Atlanta GA

^f Department of Mathematics and Statistics, Amherst College, Amherst MA

^g Division of Biomedical Sciences, Warwick Medical School, University of Warwick, Coventry, UK

^h Department of Molecular, Cell and Cancer Biology, University of Massachusetts Chan Medical School, Worcester MA

ⁱ NeuroNexus Institute, University of Massachusetts Chan Medical School, Worcester MA

¹ C.B.S and V.v.d.V. contributed equally to this work.

² Present address: American Society for Biochemistry and Molecular Biology, Rockville MD 20852

³ Present address: University of California, San Diego, La Jolla, CA USA

⁴ To whom correspondence may be addressed:

Email: David.weaver@umassmed.edu

David R. Weaver, Ph.D., Department of Neurobiology, LRB-723, UMass Chan Medical School, 364 Plantation St., Worcester MA 01605

Keywords: Circadian Rhythms, Bioluminescence, Luciferase, Misalignment, *Dbp*, Albumin D-element binding protein, *In Vivo* Imaging System (IVIS), LumiCycle *In Vivo*, Reporter Mouse, Peripheral Oscillators

Conflict of interest statement: The authors declare no conflicts of interest.

31 **Abstract**

32 Circadian rhythms are endogenously generated physiological and molecular rhythms with a cycle length of
33 about 24 h. Bioluminescent reporters have been exceptionally useful for studying circadian rhythms in
34 numerous species. Here, we report development of a reporter mouse generated by modification of a widely
35 expressed and highly rhythmic gene encoding D-site albumin promoter binding protein (*Dbp*). In this line
36 of mice, firefly luciferase is expressed from the *Dbp* locus in a *Cre*-recombinase-dependent manner,
37 allowing assessment of bioluminescence rhythms in specific cellular populations. A mouse line in which
38 luciferase expression was *Cre*-independent was also generated. The *Dbp* reporter alleles do not alter *Dbp*
39 gene expression rhythms in liver or circadian locomotor activity rhythms. *In vivo* and *ex vivo* studies show
40 the utility of the reporter alleles for monitoring rhythmicity. Our studies reveal cell-type specific
41 characteristics of rhythms among neuronal populations within the suprachiasmatic nuclei *ex vivo*. *In vivo*
42 studies show *Dbp*-driven bioluminescence rhythms in the liver of *Albumin-Cre;Dbp^{KI/+}* “liver reporter”
43 mice. After a shift of the lighting schedule, locomotor activity achieved the proper phase relationship with
44 the new lighting cycle more rapidly than hepatic bioluminescence did. As previously shown, restricting
45 food access to the daytime altered the phase of hepatic rhythmicity. Our model allowed assessment of the
46 rate of recovery from misalignment once animals were provided with food *ad libitum*. These studies
47 confirm the previously demonstrated circadian misalignment following environmental perturbations and
48 reveal the utility of this model for minimally invasive, longitudinal monitoring of rhythmicity from specific
49 mouse tissues.

50

51 Introduction

52 Circadian rhythms are endogenous rhythms with a cycle length of ~24 hours. The mammalian
53 circadian system is hierarchical, with the hypothalamic suprachiasmatic nuclei (SCN) serving as the
54 pacemaker (Mohawk et al., 2012; Herzog et al., 2017). The SCN are synchronized by environmental cues,
55 of which the light-dark cycle is the most influential. The SCN are not unique in their capacity for
56 rhythmicity, however. The transcriptional-translational feedback loop regulating molecular oscillations in
57 the SCN is also present in individual cells throughout the body (Mohawk et al., 2012). SCN-driven neural,
58 behavioral and hormonal rhythms synchronize these cell-autonomous oscillators, leading to rhythmicity
59 with predictable phase relationships among tissues, genes and physiological processes (Mohawk et al.,
60 2012; Patke et al., 2020; Zhang et al., 2014). Repeated disruption of this internal temporal order by
61 inappropriately timed light exposure or food intake leads to adverse health consequences in shift-working
62 humans and in animal models (Evans & Davidson, 2013; Patke et al., 2020). Progress in identifying the
63 mechanisms by which chronic circadian disruption leads to adverse health consequences will require long-
64 term monitoring of central and peripheral rhythms (Roenneberg & Meroow, 2016).

65 Rhythmically expressed reporter genes have been extremely important for demonstrating cell-
66 autonomous circadian clocks and monitoring rhythmicity in several organisms, including plants (Millar et
67 al., 1992), *Neurospora* (Morgan et al., 2003), cyanobacteria (Kondo et al., 1993), *Drosophila* (Brandes et
68 al., 1996), zebrafish (Weger et al., 2013), cultured cells (Nagoshi et al., 2004; Hirota et al., 2010; Welsh et
69 al., 2004; Zhang et al., 2009), rodent tissue explants (Abe et al., 2002; Maywood et al., 2013; Yamazaki et
70 al., 2000; Yoo et al., 2004; Yoo et al., 2005), and rodent tissues *in vivo* (Saini et al., 2013; Tahara et al.,
71 2012). Circadian reporter genes have been instrumental in screens to identify clock genes and modifiers in
72 many of these systems (Cesbron et al., 2013; Chen et al., 2012; Hirota et al., 2010; Kondo et al., 1993;
73 Millar et al., 1995; Muñoz-Guzmán et al., 2021; Stanewsky et al., 1998; Zhang et al., 2009). Circadian
74 reporters have also been used to assess rhythmicity in peripheral tissues and the impact of alterations in
75 experimental or environmental conditions (food availability, lighting cycles, glucocorticoid treatment) on
76 peripheral oscillators, conducted by measuring bioluminescence rhythms in tissue explants monitored *ex*

1
2
3 77 *in vivo* (Davidson et al., 2008; Davidson et al., 2009; Nakamura et al., 2005; Pezuk et al., 2012; Sellix et al.,
4
5 78 2012; Stokkan et al., 2001; Yamanaka et al., 2008; Yamazaki et al., 2000). These studies complement
6
7 79 work done by assessing population rhythms in gene expression in tissue samples indicating altered
8
9 80 rhythm amplitude and phase, and altered phase relationships in and between SCN and peripheral
10
11 81 oscillators following resetting (Balsalobre et al., 2000; Damiola et al., 2000; Destici et al., 2013; Nagano
12
13 82 et al., 2003; Reddy et al., 2002; Yamaguchi et al., 2013; for review see Nicholls et al., 2019). Several
14
15 83 groups have developed methods for *in vivo* assessment of reporter gene activity from brain regions,
16
17 84 including the SCN, using implanted optical fibers and freely moving (but tethered) rodents (Hamada et
18
19 85 al., 2016; Mei et al., 2018; Nakamura et al., 2008; Ono et al., 2015; Yamaguchi et al., 2001; Yamaguchi
20
21 86 et al., 2016). Other studies have localized the source of bioluminescence from widely expressed reporter
22
23 87 genes in specific peripheral tissues based on photomultiplier tube placement on the body surface (Hamada
24
25 88 et al., 2016; Sawai et al., 2019). Peripheral organ reporter gene activity has been assessed by *in vivo*
26
27 89 imaging in anesthetized mice (Saini et al., 2013; Tahara et al., 2012) and more recently in ambulatory
28
29 90 mice (Martin-Burgos et al., 2020; Saini et al., 2013; Sinturel et al., 2021). In some cases, viral vectors
30
31 91 that afford anatomical specificity (through their site of injection, tropism and/or by their design) have
32
33 92 been used to direct reporter expression to specific tissues (Mei et al., 2018; Saini et al., 2013; Sinturel et
34
35 93 al., 2021). All of these approaches are hampered by the need to develop specific reagents or approaches
36
37 94 for each tissue being examined, and many of these approaches are invasive. In view of the large number
38
39 95 of mouse lines with tissue-specific expression of *Cre* recombinase, the field would benefit considerably
40
41 96 from a binary (*Cre-lox*) reporter system in which bioluminescence from a rhythmically expressed gene
42
43 97 can be switched on in tissues expressing *Cre* recombinase, simply by crossing mice of the appropriate
44
45 98 genotypes together.

49 99 Here, we report a new transgenic mouse line in which firefly luciferase is expressed from the mouse
50
51 100 *Dbp* locus in a *Cre*-recombinase-dependent manner. *Dbp* is widely and rhythmically expressed (Fonjallaz
52
53 101 et al., 1996; Punia et al., 2012; Zhang et al., 2014), allowing detection of circadian bioluminescence rhythms
54
55 102 in numerous tissues, *in vivo* and *ex vivo*. *Cre*-dependent bioluminescence rhythms were recorded *ex vivo*

JBR 21-117.R1

1
2
3 103 from specific SCN neuronal populations. Furthermore, we observed transient misalignment between
4
5 104 behavioral and hepatic bioluminescence rhythms in freely moving mice subjected to a shift of the light-
6
7 105 dark cycle or following restricted food access.
8

9 106 While this work was being prepared for publication, Shan et al. (2020) reported development of a
10
11 107 Color-Switch *Per2* reporter mouse. In this reporter, *Cre* recombinase expression changes the reporter fused
12
13 108 to mPER2 from red to green luciferase.
14
15

16 109

18 110 **Materials and Methods**

19 111

23 112 **Animals and Housing Conditions**

24
25 113 All animal procedures were reviewed and approved by the Institutional Animal Care and Use
26
27 114 Committees of the University of Massachusetts Chan Medical School, Morehouse School of Medicine, the
28
29 115 University of Warwick, and/or Smith College.
30

31 116 Unless otherwise noted, animals were maintained in a 12h light: 12h dark (LD) lighting cycle with
32
33 117 access to food (Prolab Isopro RMH3000; LabDiet) and water available *ad libitum*. Zeitgeber Time (ZT)
34
35 118 refers to time relative to the lighting cycle. ZT 0-12h is the light phase and ZT 12-24h is the dark phase.
36

37 119 *Cre* recombinase-expressing lines were crossed to mice bearing the conditional (*Dbp^{Kl}*) reporter
38
39 120 allele to generate mice expressing luciferase in specific cells or tissues. *Albumin-Cre* (B6.Cg-*Speer6-*
40
41 121 *ps1^{Tg(Alb-Cre)21Mgn/J}*; JAX stock number 003574), *Ksp1.3-Cre* (B6.Cg-Tg{*Cdh16-cre*}911gr/J, JAX
42
43 122 012237), *AVP-IRES2-Cre* (B6.Cg-*Avp^{tm1.1(Cre)Hze/J}*; JAX 023530), and *NMS-Cre* mice (Tg(Nms-
44
45 123 *iCre*)^{20Ywa}, JAX 027205) were obtained from the Jackson Labs (Bar Harbor, ME). These lines direct *Cre*
46
47 124 recombinase expression to hepatocytes (Postic et al., 1999), renal tubules and genito-urinary epithelia
48
49 125 (Shao et al., 2002), neurons expressing arginine vasopressin (AVP; Harris et al., 2014), and neurons
50
51 126 expressing Neuromedin S (NMS; Lee et al., 2015), respectively. A *Prrx1-Cre* female (B6.Cg-Tg(*Prrx1-*
52
53
54
55
56
57
58
59
60

1
2
3 127 Cre^{1Cjt/J}), JAX 005584; Logan et al., 2002) was used for germline deletion of the conditional allele (see
4
5 128 below).

6
7 129 Founder *Per2^{LucSV/+}* mice with an in-frame fusion of firefly luciferase to PER2 and an SV40
8
9 130 polyadenylation signal (Welsh et al., 2004; Yoo et al., 2017) were generously provided by Dr. Joseph
10
11 131 Takahashi, University of Texas Southwestern Medical School, Dallas. All *Per2^{LucSV}* reporter mice used for
12
13 132 experiments here were heterozygous (e.g., *Per2^{LucSV/+}*). For clarity when referring to literature describing
14
15 133 the more widely used *PER2::LUCIFERASE* fusion reporter line in which the endogenous *Per2* 3' UTR is
16
17 134 downstream of the luciferase coding sequence (Yoo et al., 2004), we will refer to this line as *Per2^{Luciferase}*.
18
19 135 Mouse lines were maintained by backcrossing to the C57BL/6J (JAX 000664) background.

20
21
22 136 We also generated albino reporter mice by backcrossing to albino C57BL/6J mice with a
23
24 137 mutation in tyrosinase (*tyr/tyr*; B6(Cg)-*Tyr^{c-2J}/J*, JAX stock number 00058). Tyrosinase, like *Dbp*, is
25
26 138 located on mouse chromosome 7. Crossing these lines eventually generated a recombinant (*Dbp^{KI/+}*;
27
28 139 *tyr/tyr*) in which both mutant alleles were on the same chromatid. Subsequent crossing to albino mice
29
30 140 expressing *Cre* recombinase allowed production of albino reporter mice. Albino *Dbp^{KI/+}* mice on the
31
32 141 B6(Cg)-*Tyr^{c-2J}/J* background are being deposited in the Jackson Labs repository (Bar Harbor, ME) as
33
34 142 stock number 036997.

35
36
37 143 Note, caution is needed with the *Ksp1.3-Cre* line reported here, as it has a high frequency of
38
39 144 germline recombination (excision of the floxed region of the conditional allele in the germline, leading to
40
41 145 non-conditional luciferase expression) when *Ksp1.3-Cre* is present in the same parent as *Dbp^{KI/+}*.
42
43 146 Recombination also frequently occurs when *Ksp1.3-Cre* females are crossed with *Dbp^{KI}* males. When using
44
45 147 the *Cre/lox* system, genotyping strategies should be designed to detect all possible alleles. Even when the
46
47 148 *Ksp1.3-Cre; Dbp^{KI/+}* genotype is generated without germline excision of GFP, the sex difference in *Cre*
48
49 149 expression leads to markedly different bioluminescence patterns in males and females (see Results).

50
51
52 150

53
54 151 **CRISPR/Cas9 targeting the *Dbp* locus**

JBR 21-117.R1

1
2
3 152 The mutant allele was generated by CRISPR/Cas9 mediated engineering of the *Dbp* locus. The
4
5 153 targeting construct (**Figure 1**) consisted of a 5' homology arm terminating just 5' of the *Dbp* stop codon
6
7 154 followed by in-frame sequences encoding a T2A linker (to separate DBP protein from the reporter
8
9 155 polypeptides; Kim et al., 2011), loxP, GFP with the bovine growth hormone polyadenylation signal, loxP,
10
11 156 and *Luc2* followed by the 3'-UTR of *Dbp* (3' homology arm). In the presence of CRE recombinase, two
12
13
14 157 loxP sites oriented in the same direction will recombine, leading to deletion of the sequence between them
15
16 158 (GFP in this case).

17
18 159 In the successful set of microinjections, 34 blastocysts were injected with 40 ng/μl guide RNA
19
20 160 MmDBPki_gR49f, 50 ng/μl *Cas9* mRNA (synthesized from a *Cas9* PCR product using mMessage
21
22 161 mMachine T7 Ultra Kit from Life Technologies) and 20 ng/μl CAS9 protein (IDT). Two putative founders
23
24 162 were identified using a primer pair internal to the construct (primer pair C; **Table S1**). Additional primer
25
26 163 pairs consisting of a primer in flanking DNA (external to the construct) and a primer within the construct
27
28 164 were used to determine whether these animals had the desired targeting event (primer pairs F and H, which
29
30 165 spanned the 5' and 3' ends, respectively). These studies led to identifying one mouse as having the correct
31
32 166 insertion and recognizing that the other putative founders had random insertion of the construct rather than
33
34 167 homologous recombination into the *Dbp* locus; the mouse with random insertion was not studied further.
35
36 168 Genomic DNA from the founder with insertion into the *Dbp* locus was amplified using a primer pair
37
38 169 flanking the entire construct. Sequencing the product confirmed the construct was inserted properly, *in vivo*.
39
40 170 Primer sets used for verification of the proper insertion of the construct are listed in **Table S1**.

41
42 171 The founder carrying the targeted (knock-in or *Dbp^{KI}*) allele and its offspring were backcrossed to
43
44 172 C57BL/6J mice (JAX 000664) for three generations before any intercrossing to reduce the chance of a
45
46 173 potential off-target mutations becoming established in the reporter line.

47
48 174 To generate mice with germline deletion of GFP (and thus leading to expression of luciferase
49
50 175 throughout the body), a male *Dbp^{KI/+}* was bred to a *Prrx1-Cre* female, which we had on hand and which, in
51
52 176 our experience, produces germline deletion of floxed alleles at high frequency when CRE is introduced
53
54
55
56
57
58
59
60

177 from the female. Several mice bearing the newly generated *Dbp^{Luc}* allele were identified and backcrossed
178 to C57BL/6J mice, selecting against *Prrx1-Cre*.

179

180 **Genotyping**

181 Genotyping was performed by PCR amplification of DNA extracted from ear punches.
182 Amplification products were separated by agarose gel electrophoresis. Genotyping protocols for *Per2^{LucSV}*
183 and *Cre* recombinase have been published previously and are listed in Table S1 (van der Vinne et al., 2018;
184 Weaver et al., 2018, respectively). A mixture of four primers (primer set “4A”) capable of detecting all
185 possible *Dbp* allele combinations was used for colony genotyping; the three possible alleles (*Dbp^{KI}*, *Dbp^{Luc}*,
186 *Dbp⁺*) generate amplicons of 399, 490 and 299 bp, respectively with this primer set. Primer set 4A consists
187 of a common forward primer in exon 4 (5'-TGCTGTGCTTTCACGCTACCAGG-3') and allele-specific
188 reverse primers in GFP (to detect the *Dbp^{KI}* allele; 5'-AGTCGTGCTGCTTCATGTGGTTCG-3'), in *Luc2*
189 (to detect the *Dbp^{Luc}* allele; 5'-TCGTTGTAGATGTCGTTAGCTGG-3'), and in the *Dbp* 3' UTR (to detect
190 the unmodified *Dbp* allele; 5'-TTCAGGATTGTGTTGATGGAGGC-3').

191

192 **Generation of Digoxigenin (DIG) DNA Probes and Northern Blot Assay.**

193 DIG-labeled DNA probes were generated by PCR in reactions containing 28 μ M of DIG-labeled
194 UTP. Primer sets are listed in **Table S1**.

195 Male mice of five genotypes (WT, *Dbp^{KI/+}*, *Dbp^{KI/KI}*, *Dbp^{Luc/+}*, and *Dbp^{Luc/Luc}*) were euthanized by
196 Euthasol injection for collection of liver tissue at 4-h intervals (ZT 2, 6, 10, 14, 18, 22). RNA was isolated
197 from the liver tissue by Trizol extraction (Ambion). RNA was quantitated by Nanodrop. Five micrograms
198 per lane were separated by electrophoresis on 1.2% formaldehyde gels. RNA was transferred to nylon
199 membranes and cross-linked by UV exposure. Blots were prehybridized, probed and detected following the
200 manufacturer's protocol (Roche), bagged and exposed to X-ray film.

JBR 21-117.R1

1
2
3 201 Film images of the blots were analyzed by determining the optical density of the *Dbp* and *Actin*
4
5 202 bands within each lane and taking the *Dbp/Actin* ratio. The *Dbp/Actin* ratios were converted to percentage
6
7 203 of maximum *Dbp/Actin* for each transcript type within each blot. Due to the difference in band location of
8
9 204 the three *Dbp* alleles, heterozygous animals contributed a set of values for both the wild-type transcript and
10
11 205 the reporter transcript on each blot. Friedman's one-way analysis of variance and Dunn's test were used for
12
13 206 non-parametric assessment of differences between time-points for each transcript.
14
15
16 207

207

208 **Locomotor Activity Rhythms**

19
20 209 Male and female mice of five genotypes (WT, *Dbp*^{KI/+}, *Dbp*^{KI/KI}, *Dbp*^{Luc/+}, and *Dbp*^{Luc/Luc}) were
21
22 210 transferred to the experimental room and single-housed with a running wheel. Animals had access to food
23
24 211 and water *ad libitum*. Running-wheel activity was monitored and analysed using ClockLab collection
25
26 212 software (Actimetrics). Mice were entrained to a 12-h light/12-h dark cycle for 18 days, then were placed
27
28 213 into constant darkness (dim red light) for 15 days. The free-running period in constant darkness (DD) was
29
30 214 determined for each animal on DD days 4-15 by periodogram analysis (ClockLab).
31
32
33 215

215

216 **Bioluminescence Recordings from Tissue Explants**

34
35 216
36
37 217 Tissue explants were prepared late in the afternoon from *Per2*^{LucSV/+} and *Dbp*^{Luc/+} mice housed on a
38
39 218 12-h light/12-h dark lighting cycle. Tissues from the two genotypes were studied together in each run. Mice
40
41 219 were deeply anesthetized with Euthasol and decapitated. Tissues were dissected and immediately placed in
42
43 220 ice-cold 1X HBSS (Gibco). Pituitary gland was subdivided into 4 sections (~2mm³) with a scalpel and each
44
45 221 piece was cultured separately. Lung explants were placed three per dish. Up to three replicate dishes were
46
47 222 studied per tissue per animal. Explants were placed on sterile 35-mm Millicell culture plate inserts
48
49 223 (Millipore) in a sealed petri dish containing air-buffered bioluminescence medium (Yamazaki and
50
51 224 Takahashi, 2005) plus D-luciferin (100 μM) (Gold Biotechnology) and incubated at 32 °C as previously
52
53 225 described (van der Vinne et al., 2018). Bioluminescence in each dish was measured for 1 minute every 15
54
55 226 minutes using a Hamamatsu LM-2400 luminometer.
56
57

227 Bioluminescence records were analyzed using Microsoft Excel to determine period and peak time.
228 The first 12-h were discarded to exclude acute responses to explant preparation. Photon counts were
229 smoothed to a 3-h running average and baseline subtracted using a 24-h running average. Circadian period
230 was determined from the average of the period between each peak, trough, upward crossing and downward
231 crossing between 24 and 88 hr of recording for each record. Peak time was calculated as the clock time of
232 the first peak in the background-subtracted data and is expressed relative to ZT of the extrapolated lighting
233 cycle.

234 235 **Imaging of Bioluminescence Rhythms *In Vivo***

236 *In vivo* imaging was performed in the UMass Chan Medical School Small Animal Imaging Core
237 Facility using an *In Vivo* Imaging System (IVIS-100, Caliper, now Perkin Elmer) as previously described
238 (van der Vinne et al., 2018; van der Vinne et al., 2020). *Alb-Cre⁺; Dbp^{Kl/+}* (liver reporter), *Dbp^{Luc/+}*, and
239 *Per2^{LucSV/+}* mice were anesthetized with 2% isoflurane (Zoetis Inc.) and skin covering the liver, kidneys and
240 submandibular glands was shaved. Mice were injected with D-luciferin (i.p., 100 μ l at 7.7 mM, Gold
241 Biotechnology) and dorsal (9 min post-injection) and ventral (10.5 min post-injection) images were
242 captured. To assess bioluminescence rhythms, anesthesia, D-luciferin injection and imaging was repeated
243 at 4- to 8-hour intervals over approximately 30 hours. Similarly, female kidney reporter mice (*Ksp1.3-Cre;*
244 *Dbp^{Kl/+}*) were imaged in a separate experiment to assess rhythmicity in bioluminescence, with 5 time-points
245 distributed over 48 h. IVIS images were analyzed using Caliper Life Sciences' Living Image software
246 (version 4.4) within Regions of Interest (ROI) of fixed size.

247 Whole-body reporters (*Dbp^{Luc/+}*) and liver reporters (*Alb-Cre⁺;Dbp^{Kl/+}*) were also used to assess
248 the distribution of bioluminescence by IVIS imaging. Mice were anesthetized with isoflurane, shaved, and
249 injected with D-luciferin (100 microliters at 7-10 mM, i.p.) at times of peak expression (ZT 11-16). Images
250 were captured of ventral and dorsal views at 9-12 minutes after injection. Bioluminescent counts within
251 regions of interest (ROIs) were calculated using Living Image software. ROIs identified on the ventral
252 surface were the whole rectangular region containing the mouse, and sub-ROI's were a region in the throat

JBR 21-117.R1

253 (submandibular gland), upper abdomen, and lower abdomen. Dorsal ROI's were the rectangle containing
254 the entire mouse and a sub-ROI over the lower back, corresponding to the abdomen on the dorsal side.
255 Subsequent calculations were performed in Microsoft Excel.

256 Liver and kidney reporter mice were anesthetized, dissected and imaged to confirm that
257 bioluminescence originated exclusively from the liver. In additional animals, animals were euthanized
258 before image collection.

259

260 **Bioluminescence Imaging of SCN Explants**

261 Coronal sections containing SCN from adult *NMS-Cre;Dbp^{KI/+}*, *AVP-IRES-CRE;Dbp^{KI/+}*, and
262 *Dbp^{Luc/+}* mice were dissected, cultured, and imaged as previously described (Evans et al., 2011; Evans et
263 al., 2013). Briefly, sections containing SCN (150 μ m) were cultured on a Millicell membrane in air-buffered
264 media containing 100 μ M D-luciferin (Gold Biotechnology) and imaged for 5 days using a Stanford
265 Photonics XR/MEGA-10Z cooled intensified charge-coupled device camera.

266 Rhythmic parameters of luciferase expression were calculated for each slice and for cell-like
267 regions of interest (ROIs) within each slice using computational analyses in MATLAB (R2018a,
268 MathWorks) as described previously (Evans et al., 2013; Leise & Harrington, 2011). Briefly, to locate
269 and extract data from cell-like ROIs, we employed an iterative process identifying clusters of at least 20
270 bright pixels after background and local noise subtraction (through application of a 2D wavelet transform
271 using Wavelab 850, (<https://statweb.stanford.edu/~wavelab/>) of a slice image summed across 24 h of
272 bioluminescence. To extract time series for the ROI's, each image in the sequence was smoothed via
273 convolution with a Gaussian kernel applied to 12x12-pixel regions and reduced from 512x640 resolution
274 to 256x320. A discrete wavelet transform (DWT) was applied to each time series to remove the trend and
275 to extract the circadian and noise components using the *wmtsa* toolbox for MATLAB
276 (<https://atmos.uw.edu/~wmtsa/>). The criteria for circadian rhythmicity in the ROI time series were a peak
277 autocorrelation coefficient of at least 0.2, a circadian component peak-to-peak time between 18 and 30 h,
278 an amplitude above baseline noise (standard deviation of noise component), and a cross-correlation

1
2
3 279 coefficient of at least 0.4 with an aligned sine wave over a 48h window. Peaks of the DWT circadian
4
5 280 component were used to estimate peak time of each ROI.
6

7 281 Rhythmicity index (RI) is the peak in the autocorrelation of the DWT-detrended time series,
8
9 282 corresponding to a lag between 16 and 36 hrs, as previously described (Leise et al., 2013; Leise, 2017).
10
11 283 The time of peak bioluminescence, rhythmicity index and the scatter of peak times within each slice for
12
13 284 each ROI was assessed on the first day *ex vivo*. Period of rhythmicity in each ROI was determined as the
14
15 285 average peak-to-peak interval in the second and third cycles. These measures were compared between
16
17 286 genotypes by a general linear model, with slice ID included as a random variable to account for multiple
18
19 287 cells being measured on each slice. Where applicable, post-hoc comparisons were performed using Tukey's
20
21 288 HSD pairwise comparisons.
22
23
24
25

26 290 **Data Collection and Analysis of Bioluminescence Rhythms in Ambulatory Liver Reporter Mice**

27
28 291 Bioluminescence was measured in freely moving *Alb-Cre⁺; Dbp^{KI/+}* reporter mice with the
29
30 292 “Lumicycle *In Vivo*” system (Actimetrics, Wilmette, IL) using methods as recently described (Martin-
31
32 293 Burgos et al., 2020). Animals were checked daily at varied times using an infrared viewer (Carson OPMOD
33
34 294 DNV 1.0), or goggles (Pulsar Edge Night Vision Goggles PL75095).
35
36

37 295 Each Lumicycle *In Vivo* unit contained two PMTs (Hamamatsu H8259-01), and programmable
38
39 296 LED lights. A programmable shutter blocked the PMTs during periods of light exposure and to measure
40
41 297 ‘dark counts’. Each 1-minute dark-count value was subtracted from the counts recorded during the
42
43 298 subsequent 14 minutes to obtain the background-corrected count values, to compensate for the effect of
44
45 299 temperature fluctuations on PMT signal.
46

47 300 Ambulatory bioluminescence data were analyzed using RStudio. A discrete wavelet transform
48
49 301 (DWT) was applied to each time series to detrend and to calculate the time of peaks using the *wmtsa* R
50
51 302 package (<https://cran.r-project.org/web/packages/wmtsa/index.html>), as described (Leise & Harrington,
52
53 303 2011; Leise et al., 2013; Leise, 2017). The S12 filter was applied on 15-min median binned data; medians
54
55
56
57
58
59
60

JBR 21-117.R1

304 were used (instead of means) to reduce the effect of large outliers. Data before the first trough and after the
305 last trough were discarded to avoid edge effects.

306 Locomotor activity was recorded using passive infrared motion sensors (Viconic, K940) and
307 Clocklab software (RRID:SCR_014309). The mid-point of locomotor activity was determined by wavelet
308 analysis on each day of recording. Midpoints were used because the onset of locomotor activity is poorly
309 defined using motion sensors (relative to running wheel onsets).

310

311 **Assessing Routes of Administration of Luciferin.**

312 To determine whether rhythmic substrate intake influences the pattern of bioluminescence, we
313 compared the time of peak bioluminescence between animals receiving continuous administration of
314 substrate (from a subcutaneous osmotic minipump) with trials in which mice received D-luciferin in the
315 drinking water (2 mM) and implantation of a PBS-filled osmotic pump.

316 Liver reporter mice previously housed in 12L:12D were entrained to a skeleton photoperiod (SPP)
317 consisting of four 1-hour light pulses. A skeleton photoperiod provides additional periods of darkness in
318 which to record bioluminescence. The use of a 4-pulse SPP (rather than the more typical 2-pulse SPP) was
319 based on preliminary studies indicating a 4-pulse SPP could more consistently cause phase advances of
320 locomotor activity following an advance shift of the lighting cycle. In this 4-pulse SPP, illumination
321 occurred in four 1-hour blocks within the light phase in the preceding lighting cycle (e.g., lights were on
322 from ZT 0-1, 2-3, 9-10, and 11-12, so the first and last hours of light in SPP coincided with the first and
323 last hours of illumination in the full photocycle (with lights on ZT0-12 and lights off ZT12-24/0).

324 On the seventh day of SPP entrainment, mice were given analgesics (0.05 mg/kg Buprenorphine
325 and 2.0 mg/kg Meloxicam), anesthetized with 3% isoflurane, shaved from hips to shoulders, and a primed
326 osmotic minipump (Alzet Model #1002, 0.25 μ l per hour, 14 day) containing D-luciferin (100 mM dissolved
327 in PBS) or PBS vehicle was implanted subcutaneously. Mice were returned to their cages with a warming
328 disc and were provided soft food during the first 24 hours of recovery. Animals were placed into the
329 LumiCycle *In Vivo* unit 2.5 days after surgery. Bioluminescence was recorded in SPP lighting for 2.5 days,

1
2
3 330 then lights were disabled at the time of lights-out. The time of peak bioluminescence was determined by
4
5 331 wavelet analysis on the first day in constant darkness. No difference in peak time of bioluminescence was
6
7 332 found (see Results); in subsequent studies of ambulatory Liver reporter mice, D-luciferin (2 mM) was
8
9 333 administered in the drinking water.
10

11 334

12 13 335 **Re-entrainment following a Phase Shift of the Skeleton Photoperiod.**

14
15 336 Liver reporter mice (*Albumin-Cre; Dbp^{KI/+}*) previously entrained to LD were transferred to the
16
17 337 skeleton photoperiod for several days. Mice were anesthetized with isoflurane and shaved 2.5 days prior to
18
19 338 placement in the LumiCycle *In Vivo* units. D-Luciferin (2 mM) was provided in the drinking water. Skeleton
20
21 339 photoperiod lighting conditions were either maintained at the initial pattern or advanced by 6 hr after the
22
23 340 second day of recording. Locomotor activity was detected by passive infrared motion sensors.
24
25

26 341 The circadian time of peak bioluminescence and the mid-point of locomotor activity were
27
28 342 determined by wavelet analysis on each day of recording. We used the midpoint of locomotor activity
29
30 343 because activity onset was not easily defined using motion sensors. The timing of bioluminescence and
31
32 344 locomotor activity rhythms was normalized to the timing of these rhythms on Day 2 (e.g., the last day
33
34 345 before shifting the lighting cycle in the shifted group) for each animal. Data are expressed as mean \pm SEM
35
36 346 for each lighting condition and endpoint on each day. Data from each lighting group were analyzed
37
38 347 separately using a general linear model with Animal ID as a random variable (allowing comparison of the
39
40 348 two rhythms within individuals) and the main effects of the endpoint measure (locomotor activity or
41
42 349 bioluminescence) and Day number, and the 2-way interaction Measure*Day. In animals not undergoing a
43
44 350 phase shift, potential changes in the timing of the locomotor or bioluminescence rhythm were assessed
45
46 351 separately for either measure by testing the influence of Day number.
47
48

49 352

50 51 353 **Food Restriction Followed by Bioluminescence Recording.**

52
53 354 Liver reporter mice (*Albumin-Cre; Dbp^{KI/+}*) were fed pellets (300 mg, Dustless Precision Pellets,
54
55 355 Rodent, Grain-Based, F0170, BioServ, Flemington, NJ, USA) through the Actimetrics timed feeding
56
57

JBR 21-117.R1

1
2
3 356 apparatus designed by Phenome Technologies, Skokie, IL, USA. Pellets were spaced by a minimum of 10
4
5 357 minutes to prevent hoarding behaviour (Acosta-Rodriguez et al., 2017). Liver reporter animals were
6
7 358 randomly assigned to treatment groups and recording boxes. Three groups were studied: those with *ad*
8
9 359 *libitum* access to food, those with feeding restricted to the light phase of the LD cycle (daytime feeding),
10
11 360 and mice with access to food restricted to the dark phase of the LD cycle (nighttime feeding). Mice were
12
13 361 weighed regularly to ensure body weight did not decrease below 95% of initial weight. All mice were kept
14
15 362 on a 12L:12D lighting schedule during the period of food manipulation, and then were released into constant
16
17 363 darkness with D-luciferin (2mM) in the drinking water for bioluminescence recording. During the LD
18
19 364 period, data were collected on feeding, light levels, and locomotor behavior (using motion sensors). Three
20
21 365 days before entering the LumiCycle *In Vivo* units, cage bottoms were changed at dark onset. *Ad libitum* and
22
23 366 night-fed mice were placed into the LumiCycle *In Vivo* units at dark onset with food immediately available.
24
25 367 Day-fed mice were placed into the LumiCycle *In Vivo* units at dark onset but were provided food after 12
26
27 368 hours (at the time of light onset in the previous LD cycle) to continue the daytime feeding regime during
28
29 369 the first day of the recording period. Bioluminescence was recorded for 7 days.

30
31
32 370 Experimental groups and controls ran in parallel over five cohorts lasting 3 months. 24 hours prior
33
34 371 to placement in the recording boxes, mice were shaved from hips to shoulders on their front and back under
35
36 372 3% isoflurane and returned to their cages. Mice were provided with D-luciferin (2mM) in the drinking water
37
38 373 6 hours prior to placement into the LumiCycle *In Vivo* units, to enable instantaneous bioluminescence upon
39
40 374 recording onset.

41
42
43 375 The center of gravity (COG) of food intake was calculated for each animal for the last 5 days in
44
45 376 LD (e.g., the last 5 days of the feeding regimen). Food intake patterns were also independently assessed
46
47 377 qualitatively by four observers. These assessments led to identification of three cohorts of mice, based on
48
49 378 food intake patterns. Three mice were identified as clear outliers compared to these three cohorts based on
50
51 379 visual inspection of the food intake timing. In line with this qualitative assessment, the feeding COG of
52
53 380 each of these 3 animals was >2 h removed from the other animals in their cohort. These three animals were
54
55 381 excluded from cohort-based assessments. Peak of bioluminescence on each day was calculated by DWT

1
2
3 382 analysis as above. Missing data resulted from inability to define a time of peak bioluminescence on some
4
5 383 days. Hair regrowth contributed to loss of signal and loss of rhythm amplitude, and thus to missing data in
6
7 384 some cases.

9 385 **Data and Materials Availability**

11 386 Requests for research materials should be directed to Dr. David Weaver. Underlying data are
12
13 387 available from Dr. Weaver on request.

14 388

17 389 **Results**

20 390 **Generation of a bifunctional reporter mouse.** CRISPR/Cas9 genome editing was used to introduce a
21
22 391 bifunctional reporter into the mouse *Dbp* locus (**Fig. 1**). The reporter consists of a T2A sequence (to allow
23
24 392 expression of separate proteins from a single transcript), a destabilized, enhanced GFP (d2EGFP, hereafter
25
26 393 GFP) sequence flanked by loxP sites, and a codon optimised synthetic firefly *luciferase* (*Luc2* from
27
28 394 *Photinus pyralis*, hereafter luc). In the absence of *Cre* expression, DBP and GFP are expressed as separate
29
30 395 proteins. After CRE-mediated recombination, the floxed GFP is removed, and separate DBP and luciferase
31
32 396 proteins are expressed from the *Dbp* locus. Sequencing of genomic DNA confirmed successful generation
33
34 397 of the *Dbp^{KI}* conditional reporter allele.

36
37 398 A non-conditional reporter allele was generated by breeding to combine the conditional *Dbp^{KI}* allele
38
39 399 with *Cre*-recombinase expressed in the germline (of a female *Prrxl1-Cre* mouse), leading to germline
40
41 400 excision of GFP. We refer to this non-conditional allele, which expresses luciferase wherever *Dbp* is
42
43 401 expressed, as *Dbp^{Luc}*.

44 402

47 403 **Molecular and Behavioral Rhythms in Mice with *Dbp* Reporter Alleles.** To confirm that the
48
49 404 introduction of the reporter construct into the *Dbp* locus did not alter circadian clock function, molecular
50
51 405 and behavioral rhythms were assessed. Mice used for these analyses had either one or two copies of the

1
2
3 406 GFP-containing conditional allele (*Dbp^{KI/+}* and *Dbp^{KI/KI}*, respectively), one or two copies of the luciferase-
4
5 407 expressing allele (*Dbp^{Luc/+}* and *Dbp^{Luc/Luc}*, respectively), or were wild-type (WT) littermate controls.
6

7 408 RNA was isolated from male livers collected at 4-h intervals over 24-h in a 12L:12D (LD) lighting
8
9 409 cycle. Northern blots were prepared and probed for *Dbp* and *Actin* (loading control). As expected, the
10
11 410 transcripts from *Dbp^{KI}* and *Dbp^{Luc}* alleles migrated more slowly than the wild-type transcript (**Fig. 2A**), due
12
13 411 to inclusion of GFP and luciferase coding sequence in these transcripts, respectively, as verified by probing
14
15 412 for reporter sequences in a separate blot. Peak levels of *Dbp* expression in liver occurred at ZT10 in all
16
17 413 genotypes (**Fig. 2B, 2C**), as expected based on previous studies^{3,42,57}. For each transcript type, the *Dbp/Actin*
18
19 414 ratios were ranked within each series of 6 timepoints. These ranks differed significantly among the
20
21 415 timepoints for each transcript (Friedman's One-Way analysis of variance, $p < 0.002$), and post-hoc testing
22
23 416 indicated significantly higher rankings at ZT10 than at ZT2, ZT18 and ZT22 (Dunn's test, $p < 0.05$; Fig
24
25 417 2D-2F). These data indicate that the temporal profile of transcript expression from the *Dbp* locus was
26
27 418 unaffected by the inclusion of reporter sequences.
28
29

30 419 Heterozygous mice expressed both *Dbp* and *Dbp-plus-reporter* transcripts. The two transcript types
31
32 420 did not differ in abundance: optical density over film background of the *Dbp^{KI}* transcript was 100.5 ± 5.3 %
33
34 421 of the *Dbp⁺* transcript in *Dbp^{KI/+}* mice ($t=0.084$, $df=7$, $p=0.94$, one-sample t-test vs 100%), while the *Dbp^{Luc}*
35
36 422 transcript was 102.3 ± 5.0 % of *Dbp⁺* transcript in *Dbp^{Luc/+}* mice ($t=0.446$, $df=7$, $p=0.669$). The equivalent
37
38 423 expression level of the two transcript types in heterozygous animals strongly suggests that transcript
39
40 424 regulation and stability were not altered by inclusion of reporter-encoding sequences.
41
42

43 425 Locomotor activity rhythms were assessed in constant darkness in mice of both sexes in the same
44
45 426 five genotypes (**Table 1; Fig. S1**). We found a significant sex-by-genotype interaction ($F_{4,102} = 2.904$, $p =$
46
47 427 0.0254). Post-hoc tests indicated an unexpected sex difference in the *Dbp^{Luc/Luc}* mice. Indeed, when this
48
49 428 genotype was excluded from the analysis, no significant sex-by-genotype interaction was observed ($F_{3,88} =$
50
51 429 1.349 ; $p = 0.2636$) and one-way ANOVA did not find a significant main effect of genotype ($F_{3,91} = 1.174$;
52
53 430 $p = 0.3242$). One-way ANOVA within each sex with all five genotypes included revealed no genotype
54
55 431 effect in males ($F_{4,50} = 1.299$, $p = 0.283$). While there was a significant genotype effect in females ($F_{4,52} =$

432 2.716, $p = 0.040$), Tukey HSD post-hoc tests did not find a significant result among any of the pairwise
433 genotype comparisons (all p values > 0.05). Similarly, an alternative post-hoc analysis revealed that none
434 of the other female genotypes differed from WT females in their free-running period in constant darkness
435 (Dunnett's test, $p > 0.5$ in each case). To further examine the effect of sex on free-running period, males
436 and females of each genotype were compared directly. In both $Dbp^{Luc/Luc}$ and $Dbp^{KI/KI}$ mice, males had
437 significantly longer periods than females ($p < 0.01$), while there was no sex difference in wild-types or
438 heterozygous reporters ($p > 0.46$).

439 Together, these assessments of molecular and behavioral rhythms indicate that the reporter alleles
440 do not change Dbp expression or appreciably alter circadian function.

441
442 **GFP expression from the Dbp^{KI} allele.** To examine expression of GFP from the conditional allele, $Dbp^{KI/+}$
443 mice (n=5-6 mice per time-point) were anesthetized and perfused with fixative at 4-h intervals over 24 h
444 (**Fig. S2**). Liver sections from $Dbp^{KI/+}$ and control (WT) mice were examined by confocal microscopy.
445 Fluorescence signal intensity did not differ between time-points (ANOVA $F_{5,26} = 1.279$, $p = 0.7560$). GFP
446 signal from $Dbp^{KI/+}$ liver sections was 5-10x higher than from WT sections, but absolute levels were quite
447 low. The low level of GFP expression may be due to the use of destabilized GFP with a 2-hour half-life,
448 intended to more accurately track changes on a circadian time-scale. The relatively low level and lack of
449 detectable rhythmicity in GFP expression was unexpected, especially considering that liver is the tissue
450 with the highest levels of Dbp expression (Fonjallaz et al., 1996) and thus may represent a 'best-case'
451 scenario. As the primary objective of this project was to generate a mouse model with Cre -dependent
452 expression of bioluminescence from the Dbp locus, however, the absence of robust GFP-driven
453 fluorescence rhythms in Cre -negative cells did not preclude achieving this objective. GFP is effectively
454 serving as a 'floxed stop' to make luciferase expression from the Dbp locus exclusively Cre -dependent.

455
456 **Non-conditional luciferase expression from the Dbp^{Luc} allele.** The Dbp^{Luc} allele produces widespread,
457 rhythmic luciferase expression, both *in vivo* and *ex vivo*. More specifically, explants of lung and anterior

JBR 21-117.R1

1
2
3 458 pituitary gland from *Dbp^{Luc/+}* mice incubated with D-luciferin had robust circadian rhythms in
4
5 459 bioluminescence (**Fig. 3**). Furthermore, *in vivo* imaging of *Dbp^{Luc/+}* mice at 7 time-points over a ~30-h
6
7 460 period revealed rhythmic bioluminescence in the abdomen and throat in ventral views, and in the lower
8
9 461 back in dorsal views (**Fig. 4B**), similar to the distribution of bioluminescence signal from *Per2^{Luciferase/+}*
10
11 462 (Tahara et al., 2012) and *Per2^{LucSV/+}* mice (van der Vinne et al., 2018; van der Vinne et al., 2020) (**Fig. 4A**).
12
13 463 The level of light output was ~2.5-fold greater in ventral views than in dorsal views ($p < 0.0001$, Wilcoxon
14
15 464 matched pairs test, $W = 151$, $n = 17$). In the abdomen, a rostral (“liver”) region of interest (ROI) accounted
16
17 465 for $46.6 \pm 3.0\%$ (Mean \pm SEM; $n = 17$) of bioluminescence from the ventral view, while the lower abdomen
18
19 466 contributed another $38.4 \pm 3.5\%$. Bioluminescence rhythms from the throat region of *Per2^{Luciferase}* mice have
20
21 467 previously been shown to originate in the submandibular gland (Tahara et al., 2012). Bioluminescence was
22
23 468 absent in mice with wild-type *Dbp* alleles or with the conditional *Dbp^{KI}* allele (in the absence of *Cre*).
24
25

26 469 Previous reports have shown that in a number of tissues, *Dbp* RNA levels peak earlier than *Per2*
27
28 470 RNA levels (Punia et al., 2012; Zhang et al., 2014). Consistent with this literature, the time of peak of
29
30 471 bioluminescence rhythms from *Dbp^{Luc/+}* tissues preceded the time of peak of bioluminescence rhythms from
31
32 472 *Per2^{LucSV/+}* tissues by ~ 6 hours in explants (**Fig. 3C, 3F**) and by ~ 9 hr *in vivo* (**Fig. 4G-4I**).
33
34 473 Bioluminescence rhythms from *Per2^{LucSV/+}* tissue explants had significantly longer period than explants
35
36 474 from *Dbp^{Luc/+}* mice (Lung: 25.29 ± 0.13 vs 23.93 ± 0.11 h; $F_{1,27.7} = 95.55$, $p < 0.0001$; Anterior Pituitary:
37
38 475 25.27 ± 0.08 vs 23.73 ± 0.112 h; $F_{1,24.53} = 66.12$, $p < 0.0001$).
39
40
41 476

42
43 477 **Cre-dependent Luciferase Expression in Liver.** The main use we envision for the *Dbp* reporter alleles
44
45 478 involve *Cre* recombinase-mediated excision of GFP, leading to expression of *luciferase* in cells expressing
46
47 479 *Cre*. The effectiveness of this approach was first assessed in hepatocytes using an *Albumin-Cre*-driver line.
48
49 480 *In vivo* bioluminescence imaging of intact *Albumin-Cre⁺*; *Dbp^{KI/+}* “liver reporter” mice at the time of
50
51 481 expected maximal bioluminescence revealed that $96.6 \pm 0.48\%$ of light originated in the “liver” ROI
52
53 482 (relative to total ventral-view bioluminescence; $p < 0.0001$ versus $46.6 \pm 3.0\%$ in *Dbp^{Luc}* mice, U-test, $U = 0$,
54
55
56
57
58
59
60

1
2
3 483 n=19 and 17, respectively). Notably, post-mortem imaging after dissection confirmed that bioluminescence
4
5 484 originated exclusively from the liver in these mice (97.4% of light from liver; n=12).
6

7 485 In a separate cohort of liver reporter mice, bioluminescence was assessed around the clock by IVIS
8
9 486 imaging. The cosinor-fitted time of peak of *Dbp*-driven bioluminescence rhythms from the liver ‘region of
10
11 487 interest’ of these mice (ZT11) was indistinguishable from the peak time of the liver ROI analyzed in whole-
12
13 488 body *Dbp^{Luc}* mice (**Fig. 4I**).
14

15 489
16
17
18 490 **Cre-dependent Luciferase Expression in Kidney.** Viral introduction of rhythmic luciferase reporters to
19
20 491 the liver has been used previously (Saini et al., 2013, Sinturel et al., 2021), so our success with detecting
21
22 492 bioluminescence rhythms specifically from the liver in *Albumin-Cre⁺*; *Dbp^{KI/+}* “liver reporter” mice was
23
24 493 reassuring, but not surprising. With reporter genes expressing from multiple tissues (e.g., *Dbp^{Luc}* and
25
26 494 *Per2^{Luc}*), the contribution made by surrounding organs may be unclear. To extend our demonstration of
27
28 495 tissue-specific luciferase expression from the conditional *Dbp^{KI}* allele, we examined bioluminescence from
29
30 496 anesthetized *Ksp1.3-Cre*; *Dbp^{KI/+}* “kidney reporter” mice. The *Ksp1.3-Cre* driver leads to recombination in
31
32 497 the developing kidney and urogenital tissues, and in renal tubules of adult mice. In male kidney reporter
33
34 498 mice, IVIS imaging of anesthetized, dissected living mice revealed bioluminescence from the kidney and
35
36 499 seminal vesicles *in situ* (**Fig. S3, S4**). In females, bioluminescence originated from the kidney and proximal
37
38 500 ureter (**Fig. S5**). We thus used female mice to assess rhythmicity. Clear diurnal rhythmicity in
39
40 501 bioluminescence was apparent from the kidney (Friedman’s One-Way Analysis of Variance, ($F_r = 32.71$,
41
42 502 $k=5$, $n=9$, $p<0.0001$, see **Fig. S6**), with a peak at ZT8. Dunn’s test revealed that ZT8 timepoint differed
43
44 503 significantly from ZT0 and ZT18 but not from ZT4 and ZT14 (multiplicity-corrected, two-tailed Dunn’s
45
46 504 test; see **Fig. S6**).
47
48
49

50 505
51
52 506 **Cell-type Specific Bioluminescence Rhythms in SCN Slices.** The heterogeneity of SCN neurons has
53
54 507 important functional implications for our understanding of the central circadian clock (Herzog et al., 2017).
55
56 508 Neuromedin S (NMS) is expressed in ~40% of SCN cells, while Arginine Vasopressin (AVP) is expressed
57

JBR 21-117.R1

1
2
3 509 in ~10% of SCN neurons and is contained within the NMS-expressing population (Lee et al., 2015). The
4
5 510 utility of our conditional reporter line was demonstrated by monitoring bioluminescence rhythms within
6
7 511 specific subpopulations of SCN neurons (**Fig. 5**). *NMS-iCre; Dbp^{KI/+}* mice and *AVP-IRES2-Cre; Dbp^{KI/+}*
8
9 512 mice were generated, and single-cell bioluminescence rhythms were compared to those from non-
10
11 513 conditional *Dbp^{Luc/+}* mice in SCN slices *ex vivo*. For the conditional mice, bioluminescence was apparent
12
13 514 in subsets of cells within the SCN (**Fig. 5A**). The anatomical pattern of bioluminescence in the SCN differed
14
15 515 based on the *Cre* line used, consistent with the expected distribution for each neuronal subtype. In each
16
17 516 slice, rhythmic ROI's were readily apparent (**Fig. 5B**).

18
19
20 517 The cell-type specificity of bioluminescence signals from the different genotypes enabled the
21
22 518 assessment of rhythm quality in the different neural populations. This assessment revealed a significantly
23
24 519 shorter period in AVP⁺ cells compared to NMS⁺ cells (**Fig. 5C, Fig. 5D**; $F_{2,14.64} = 4.259, p = 0.0345$). The
25
26 520 time of peak of *Dbp*-driven bioluminescence did not differ significantly between the different cellular
27
28 521 populations examined (**Fig. 5E**; $F_{2,18.31} = 0.6570, p = 0.5302$), while a reduction in rhythm robustness was
29
30 522 observed in AVP⁺ neurons compared to rhythms of NMS⁺ neurons as well as compared to all cells (**Fig.**
31
32 523 **5F**; $F_{2,18.11} = 14.34, p = 0.0002$). The distribution of peak times was also more dispersed in AVP⁺ cells
33
34 524 compared to NMS⁺ cells (**Fig. 5G**).

35
36
37 525 These results complement the recent report from Shan *et al.* (2020) using a *Cre*-dependent Color-
38
39 526 Switch PER2::LUC reporter mouse demonstrating period and phase differences among sub-populations of
40
41 527 SCN neurons. Our *Dbp^{KI}* mice and the recently reported Color-Switch PER2::LUC mouse line (Shan *et al.*,
42
43 528 2020) will be important additions to our molecular-genetic armamentarium for unravelling the complicated
44
45 529 relationships among the cellular components of the SCN circadian pacemaker⁵⁸⁻⁶⁴.

530

531 **Route of Substrate Administration.**

52
53 532 **Monitoring peripheral organ circadian phase following disruptive environmental, surgical or**
54
55 533 **genetic conditions will require long-term monitoring of peripheral rhythms in ambulatory mice. Studies**
56
57 534 **using substrate delivery by mini-osmotic pump or infusion pump allow constant substrate administration**

1
2
3 535 but require surgery and, in the case of mini-osmotic pumps, are limited by the pump volume. Therefore,
4
5 536 administration of luciferase substrate in the drinking water would be preferable. Thus, we examined the
6
7 537 potential impact of route of substrate administration on rhythm phase using the Lumicycle *In Vivo* system
8
9 538 (Actimetrics, Wilmette IL) in *Albumin-Cre; Dbp^{Kl/+}* (“liver reporter”) mice. Mice were entrained to LD
10
11 539 followed by a skeleton photoperiod consisting of four 1-h pulses of light every 24 hr
12
13 540 (1L:1D:1L:6D:1L:1D:1L:12D) with the 12-h dark phase coinciding with 12-h dark phase of the preceding
14
15 541 LD cycle. A skeleton photoperiod was used because detection of bioluminescence requires the absence of
16
17 542 ambient light, while studies of light-induced phase shifting obviously require light; a skeleton photoperiod
18
19 543 is a compromise between these conflicting constraints. After 7 days in the skeleton photoperiod, mice were
20
21 544 anesthetized for subcutaneous implantation of a primed osmotic minipump (Alzet, Model #1002 (0.25µl
22
23 545 per hour)) containing either D-luciferin (100 mM) or phosphate buffered saline (PBS). Mice with PBS-
24
25 546 containing pumps received D-luciferin in the drinking water (2 mM). Rhythms of bioluminescence were
26
27 547 readily detected under these conditions (Fig. S7). The time of peak bioluminescence was determined by
28
29 548 discrete wavelet transform (DWT) analysis on the first day of exposure to constant darkness (5 days after
30
31 549 pump implantation). There was no difference in time of peak between these routes of administration
32
33 550 (drinking water: mean peak time (± SEM) CT 8.75 ± 0.20 (n = 7); osmotic minipumps: mean peak time CT
34
35 551 8.76 ± 0.19 (n=7); unpaired t-test, t = 0.0342, df = 12, p = 0.9733). Thus, the presumed rhythm of substrate
36
37 552 intake, secondary to the rhythm of water intake, does not change the time of peak of the bioluminescence
38
39 553 rhythm. This is consistent with recent results from Sinturel et al., (2021) and Martin-Burgos et al., (2022)
40
41 554 using PER2^{Luciferase} mice. Subsequent studies used D-luciferin (2 mM) administered in the drinking water.
42
43 555
44
45
46
47 556 **Circadian Misalignment Following a Phase Shift of the Lighting Cycle**. The approach described above
48
49 557 provides an unparalleled system for assessing the timing of rhythmicity in a specific tissue over long periods
50
51 558 of time. Next, hepatic bioluminescence rhythms were monitored in *Albumin-Cre; Dbp^{Kl/+}* (liver reporter)
52
53 559 mice before and after a 6-hr phase advance of the skeleton lighting cycle. Mice that remained in the original
54
55 560 (non-shifted) skeleton lighting regimen had a stable phase of hepatic bioluminescence (Fig. 6C). In contrast,

JBR 21-117.R1

1
2
3 561 mice exposed to a phase-advance of the skeleton photoperiod displayed a gradual phase-advance in both
4
5 562 locomotor activity and hepatic bioluminescence rhythms (**Fig. 6A, B**). Notably, locomotor rhythms shifted
6
7 563 more rapidly than hepatic bioluminescence (**Fig. 6B**). To compare the re-entrainment of bioluminescence
8
9 564 and locomotor activity rhythms, peak time for each rhythm each day was normalized to the time of peak on
10
11 565 the last day before shifting the lighting cycle in the shifted group (e.g., Day 2 in **Fig. 6**) for each animal.
12
13 566 Data from each lighting group were analyzed separately using a general linear model with Animal ID as a
14
15 567 random variable (allowing comparison of the two rhythms within individuals) and the main effects were
16
17 568 endpoint (locomotor activity or bioluminescence) and Day number. In animals not undergoing a phase shift,
18
19 569 the phase relationship of these endpoints was unchanged over time ($F < 1.1, p > 0.39$). In contrast, in animals
20
21 570 exposed to a 6-hr phase advance, the phase relationship of the locomotor activity and bioluminescence
22
23 571 rhythms differed significantly (Measure*Day interaction, $F_{9,54.98} = 3.358, p = 0.0024$). Post-hoc testing
24
25 572 revealed a significant difference in phase between the two measures on day 9 (Tukey HSD, $p < 0.05$). A
26
27 573 separate analysis to compare phase (relative to Day 2 baseline) between bioluminescence and locomotor
28
29 574 activity rhythms revealed significant differences between the two measures on days 5, 6, 7, 8, 9 and 10 (t-
30
31 575 tests on each day, $p < 0.05$). Thus, both locomotor activity and hepatic bioluminescence rhythms shifted
32
33 576 following a phase shift of the lighting cycle, but the rhythms differ in their kinetics of re-adjustment: liver
34
35 577 lagged behind. These data provide clear evidence for misalignment of SCN-driven behavioral rhythms and
36
37 578 hepatic rhythmicity.
38
39
40
41
42

43 580 **Recovery from Circadian Misalignment Induced by Temporally Restricted Feeding.** We next
44
45 581 conducted a study to examine misalignment induced by restricted feeding. Previous studies have shown
46
47 582 that food availability limited to daytime significantly alters phase of peripheral oscillators (Damiola et al.,
48
49 583 2000; Hara et al., 2001; Stokkan et al., 2001; Saini et al., 2013). Due to our desire to study bioluminescence
50
51 584 rhythms without interference from the LD cycle, we administered different feeding regimens in an LD cycle
52
53 585 and then assessed the hepatic bioluminescence rhythm after release to DD with *ad libitum* food. This
54
55 586 allowed us to determine the time of peak bioluminescence of the liver after restricted feeding, and the
56
57
58
59
60

1
2
3 587 opportunity to continuously observe its return toward a normal phase relationship with SCN-driven
4
5 588 behavioral rhythms over time.

6
7 589 *Alb-Cre;Dbp^{KI/+}* liver reporter mice were exposed to one of three feeding regimes (*ad libitum*,
8
9 590 nighttime, or daytime food availability; **Fig. 7A**) for ten days in LD before recording bioluminescence in
10
11 591 DD with *ad libitum* food availability. A previously described automated feeder system (Acosta-Rodriguez
12
13 et al., 2017) was used to restrict food availability. This system limits total daily consumption (to prevent
14 592 hoarding) and restricted food pellet delivery for day-fed mice to 0600-1800 h (ZT0-ZT12), and for night-
15
16 593 fed mice to 1800-0600 h ZT12 – ZT24/0). With the setting used, the system restored daily food allotments
17
18 594 to *ad libitum* fed and night-fed mice daily at 0000h (ZT18), resulting in unusual temporal profiles of food
19
20 595 intake in *ad libitum* and night-fed mice. Nevertheless, *ad libitum* and nighttime food access both resulted
21
22 596 in food intake being concentrated in the night, while daytime food availability resulted in the midpoint of
23
24 597 food intake occurring during the first half of the light phase (**Fig. 7A, 7B, 7C**). Within-group variability in
25
26 598 the timing of food intake was low except for three clear outliers (**Fig. 7C**) that were excluded from
27
28 599 subsequent analyses.
29
30 600

31
32 601 *Ad libitum* fed mice showed consistently phased rhythms in bioluminescence after transfer to DD
33
34 602 from LD, as did night-fed animals (**Fig. 7A, 7D**). In contrast, mice fed only during the light period for 10
35
36 603 days prior to housing in DD with *ad libitum* food had an earlier peak time of the hepatic bioluminescence
37
38 604 rhythm. Daytime feeding resulted in a significantly advanced peak time compared to both night-fed and *ad*
39
40 605 *libitum* fed mice, while these latter groups were statistically indistinguishable ($F_{2,259,6} = 76.66, p < 0.0001$;
41
42 606 **Fig. 7D**). Subsequent exposure to DD with *ad libitum* feeding allowed the hepatic clock of day-fed mice to
43
44 607 return toward the appropriate phase relationship with the locomotor activity rhythm.
45
46 608

47 609 Although daytime feeding resulted in an advanced time of peak bioluminescence, the timing of the
48
49 610 liver bioluminescence rhythm was not solely controlled by the timing of food intake. First, no significant
50
51 611 correlations between the timing of food intake and time of peak bioluminescence were observed within any
52
53 612 of the three feeding regimes ($F < 1.13, p > 0.32$; **Fig. 7C**). Second, the relationship between the timing of
54
55
56 612 liver bioluminescence rhythms relative to the midpoint of food intake was significantly different between
57
58
59
60

JBR 21-117.R1

1
2
3 613 the different groups ($F_{2,17} = 313.2$, $p < 0.0001$; **Fig. 7E**). While *Dbp*-driven hepatic bioluminescence
4
5 614 rhythms were roughly in anti-phase with the midpoint of feeding in *ad libitum* and night-fed mice, daytime
6
7 615 feeding resulted in near synchrony between these rhythms (**Fig. 7E**). Furthermore, although the average
8
9 616 midpoint of feeding was significantly earlier in night-fed compared to *ad libitum* fed mice ($t_{10} = 6.21$, $p <$
10
11 617 0.0001 ; **Fig. 7C**), no significant difference was observed in bioluminescence phase relative to the preceding
12
13 618 light-dark cycle (**Fig. 7D**), with the timing of liver bioluminescence rhythms relative to the midpoint of
14
15 619 food intake being significantly delayed in night-fed compared to *ad libitum* fed mice (**Fig. 7E**). Overall,
16
17 620 these results demonstrate that although the timing of food intake strongly influences liver rhythms, the
18
19 621 timing of bioluminescence rhythmicity in liver reporter mice is not solely driven by the timing of food
20
21 622 intake (with food intake regulated for this duration and in this way).
22
23
24
25

623

624 Discussion

26
27
28 625 Numerous studies have made use of rhythmically expressed bioluminescent reporter genes to
29
30 626 monitor circadian rhythms. The *Per2^{Luciferase}* mouse and other reporters with bioluminescence under the
31
32 627 control of a clock gene have been especially useful as they generate robust bioluminescence rhythms from
33
34 628 numerous tissues recorded *ex vivo* (Abe et al., 2002; Maywood et al., 2013; Yakazami et al., 2000;
35
36 629 Yamazaki and Takahashi, 2005; Yoo et al 2004; Yoo et al., 2005). The widespread expression of
37
38 630 PER2::LUCIFERASE (and other ‘non-conditional’ bioluminescence reporters) comes at a cost, however,
39
40 631 as it is not possible to assess rhythmicity in specific cell populations within a larger tissue without
41
42 632 dissection. Tissue explant preparation can cause phase-resetting, however, especially after exposure to
43
44 633 phase shifting stimuli (Noguchi et al., 2020; Leise et al., 2020). Furthermore, *ex vivo* culturing of tissues
45
46 634 does not allow assessment of rhythmicity in the context of the hierarchical circadian system or dynamic
47
48 635 changes during environmentally-induced resetting.
49
50

51
52 636 Addressing issues of internal desynchrony and misalignment of oscillators requires monitoring the
53
54 637 dynamics of tissue resetting over time after a phase-shifting stimulus. The use of *in vivo* bioluminescence
55
56 638 imaging for repeated assessments of organ-level regions of interest over multiple days is feasible but
57
58
59
60

1
2
3 639 requires several potentially disruptive anesthesia sessions (Poulsen et al., 2018) per circadian cycle. As a
4
5 640 result, *in vivo* bioluminescence imaging has generally been relegated to assessing phase of reporter gene
6
7 641 oscillations on relatively few occasions after a shifting stimulus, with rare exception (van der Vinne et al.,
8
9 642 2020). Other methods for monitoring bioluminescence and fluorescence rhythms in ambulatory mice have
10
11 643 been developed (Hamada et al., 2016; Mei et al., 2018; Nakamura et al., 2008; Ono et al., 2015; Saini et al.,
12
13 644 2013; Sawai et al., 2019; Yamaguchi et al., 2016; Yamaguchi et al., 2001), but a less invasive approach for
14
15 645 assessing rhythms in a variety of specific tissues is desirable. Notably, several abdominal organs emit
16
17 646 significant amounts of bioluminescence in “whole-body” reporter mice, including liver, kidney and
18
19 647 intestines. These tissues likely overshadow (or, more accurately, out-glow) surrounding tissues.
20
21 648 Bioluminescence from even larger organs like liver and kidney is likely ‘contaminated’ by light from
22
23 649 adjacent structures. Indeed, the size and shape of the “liver” ROI seen by IVIS imaging (Fig. 4) differs
24
25 650 between *Dbp* liver reporter mice and whole-body reporter *Dbp^{Luc}* mice. These considerations underline the
26
27 651 benefits of generating a *Cre*-conditional reporter mouse in which recombination leading to bioluminescence
28
29 652 can be directed to specific tissues and cell types.
30
31

32
33 653 We chose to modify the *Dbp* gene to generate a conditional reporter for several reasons. *Dbp* is
34
35 654 widely and rhythmically expressed at readily detectable levels (Fonjallaz et al., 1996; Punia et al., 2012;
36
37 655 Zhang et al., 2014). This feature ensures that the reporter mouse would be useful for detecting rhythmicity
38
39 656 in numerous tissues. In addition, individual clock genes are responsive to different signaling pathways. This
40
41 657 differential regulation can lead to circadian misalignment *within* the circadian clock (Reddy et al., 2002;
42
43 658 Nicholls et al., 2019). As an output gene controlled by the CLOCK:BMAL1 transcriptional activator
44
45 659 complex (Ripperger & Schibler 2006; Stratmann et al., 2012), *Dbp* rhythmicity is likely a good proxy for
46
47 660 the integrated output of the molecular clockwork. Additional *cis*-acting elements regulating *Dbp* expression
48
49 661 have been identified, however. Binding of hnRNP K to a poly-(C) motif in the proximal promoter has been
50
51 662 implicated in high-amplitude expression of *Dbp* (Kwon et al., 2019; Kwon et al., 2020). Interestingly, *Dbp*
52
53 663 appears to be insensitive to acute regulation by activation of signal transduction pathways. Unlike *Per1* and
54
55 664 *Per2*, *Dbp* gene expression is not increased in the mouse SCN following exposure to light at night (Yan et

JBR 21-117.R1

1
2
3 665 al., 2000). Furthermore, *Dbp* expression is not acutely increased by horse serum or stimulation of the
4
5 666 cAMP/PKA pathway by forskolin, which rapidly induce *Per1* (Yagita & Okamura, 1999) and
6
7 667 resynchronize molecular rhythms. Thus, *Dbp* expression and the *Dbp*-based reporter are likely to represent
8
9 668 the status of the molecular clock without interference by other influences. Finally, concern that the targeting
10
11 669 event could disrupt function of the modified gene led us to steer away from core clock genes. Mice
12
13 670 homozygous for a targeted allele of *Dbp* have only a modest circadian phenotype (Lopez-Molina et al.,
14
15 671 1997). Homozygotes of both the *Per2^{LucSV}* and *Per2^{Luciferase}* lines have altered circadian rhythms (Ralph et
16
17 672 al., 2020; Yoo et al., 2017; see below). The GFP-expressing *Dbp* transcript lacks the native 3' UTR and
18
19 673 uses an exogenous polyadenylation sequence, which could affect *Dbp* gene expression and regulation.
20
21 674 Notably, however, our Northern blot analysis suggests little or no alteration in expression level or dynamics
22
23 675 of the *Dbp* reporter transcripts.

26 676 Yoo et al. (2017) reported that homozygous *Per2^{LucSV/LucSV}* mice (in which a SV40 polyadenylation
27
28 677 site is used instead of the endogenous *Per2* 3' UTR) have a longer period length of locomotor activity
29
30 678 rhythms in DD and explant bioluminescence rhythms *ex vivo* than the more widely used *Per2^{Luciferase}*
31
32 679 reporter. The potential impact of a single *Per2^{LucSV}* allele (as used in our studies) on period length has not
33
34 680 been reported, but this could contribute to the longer period of *Per2^{LucSV/+}* explants, relative to *Dbp^{Luc/+}*
35
36 681 explants. Interestingly, Ralph et al., (2020) recently reported that the *Per2^{Luciferase}* reporter that uses the
37
38 682 endogenous *Per2* 3'UTR (Yoo et al., 2004) also has longer period in DD and other circadian phenotypes.
39
40 683 Tosini and colleagues have also recently reported retinal degeneration and alterations in classical
41
42 684 photoreception in aged male *Per2^{Luciferase/Luciferase}* mice (Goyal et al., 2021).

45 685 Shan et al. (2020) recently reported development of a Color-Switch PER2::LUC line which was
46
47 686 used to demonstrate the utility of a *Cre*-dependent reporter approach for interrogating SCN circuitry. The
48
49 687 Color-Switch PER2::Luc line has the advantage of reporting on both *Cre*-positive and *Cre*-negative cells in
50
51 688 different colors. Detection of bioluminescence from the Color-Switch PER2::LUC reporter requires
52
53 689 segmentation of the bioluminescence signal between wavelengths. Our 'simpler' approach of only inducing

1
2
3 690 a bioluminescence signal in *Cre*-positive cells of *Dbp^{KI/+}* mice enables recording of bioluminescence
4
5 691 rhythms without the need for wavelength segmentation. In addition, the *Dbp* reporter can easily be used in
6
7 692 *Per2* mutant mice. Like the Color-Switch PER2::LUC line, our *Dbp* conditional reporter line is useful for
8
9 693 *ex vivo* studies, allowing specific cellular populations to be monitored by crossing to the appropriate *Cre*-
10
11 694 expressing lines.

13
14 695 As with the Color-Switch PER2::LUC line, we also intended to generate a bifunctional reporter.
15
16 696 The inability to readily detect a GFP fluorescence rhythm in *Dbp^{KI/+}* mouse SCN or liver was unexpected.
17
18 697 It is important to emphasize that there was detectable fluorescence above baseline, but rhythmicity was
19
20 698 not detected. This could nevertheless be due in part to low signal-to-noise ratio. It is possible that the
21
22 699 short half-life of destabilized GFP, combined with the waveform of *Dbp* gene expression (being less
23
24 700 sinusoidal than the rhythms of *Per1* and *Per2*, for example) contributed to a short period of production
25
26 701 and rapid degradation of the GFP. Notably, a transgenic mouse in which a similarly destabilized GFP is
27
28 702 driven by the *Per1* promoter generates nice SCN fluorescence rhythms (Kuhlman et al., 2000). Similarly,
29
30 703 destabilized versions of VENUS (a yellow fluorescent protein) and DsRED inserted at the start codon of
31
32 704 PER1 and PER2, respectively, in bacterial artificial chromosomes have been useful for monitoring
33
34 705 rhythmic gene expression in SCN of transgenic mice (Cheng et al., 2009). Assessing immunoreactive
35
36 706 GFP (rather than native fluorescence from GFP) in the *Dbp^{KI/+}* or *Dbp^{KI/KI}* mice may improve signal
37
38 707 detection (but at the cost of real-time reporting).

39
40
41 708 It is possible that a different design of the reporter construct would have led to better success.
42
43 709 Addition of a nuclear localization signal (as done by Cheng et al., 2009) would reduce the volume in
44
45 710 which GFP is distributed, making signal intensity greater (but we note that Kuhlman et al., 2000 did not
46
47 711 incorporate an NLS into their reporter sequence). Alternatively, generating non-destabilized GFP as a
48
49 712 fusion protein with DBP might have been more successful; in this scenario, the stability of DBP would
50
51 713 regulate the stability of GFP. This fusion strategy has been used successfully with fluorescent reporters of
52
53 714 PER2 and BMAL1 (Smyllie et al., 2016; Yang et al., 2020). Another potential variation is to use

JBR 21-117.R1

1
2
3 715 fluorescent proteins other than GFP. Other fluorescent proteins may be brighter and thus more amenable
4
5 716 to this type of study.

6
7 717 Our studies reveal subtle differences among the population of oscillators defined by *AVP-Cre*,
8
9 718 *NMS-Cre*, and the entire SCN cohort. More specifically, AVP cells had a shorter period, reduced
10
11 719 rhythmicity index, and larger within-slice dispersal of peak times than the NMS cell population with which
12
13 720 it overlaps. Our results suggest that AVP cells are coordinated less well and are less robust than other
14
15 721 populations in the SCN. This suggestion is in contrast to the typical view of AVP cells as high-amplitude
16
17 722 ‘output’ neurons that also contribute to determination of period and rhythm amplitude (Herzog et al., 2017;
18
19 723 Mieda et al., 2015; Mieda et al., 2016). One possible explanation for this is that AVP is dysregulated in the
20
21 724 *Avp-Cre* line (Cheng et al., 2019), which may influence the function of the SCN as a whole in the *AVP-*
22
23 725 *IRES-Cre; Dbp^{KI/+}* genotype used here. Using an *Avp-IRES-Cre* line which does not reduce AVP
24
25 726 expression, Shan et al. (2020) reported that AVP-expressing SCN neurons have shorter period
26
27 727 bioluminescence rhythms, compared to the non-AVP cells. This contrasts directly with our finding of longer
28
29 728 period in AVP cells reporting luciferase from the *Dbp* locus. The AVP neuronal population is contained
30
31 729 entirely within the NMS-expressing population in the SCN. There is no evidence that the *Nms-Cre* line
32
33 730 alters circadian timekeeping on its own (Lee et al., 2015). The *Nms-Cre* line and the *Avp-IRES-Cre* line
34
35 731 used by Shan et al. (2020) appear to be preferable models to the *AVP-IRES-Cre* line (JAX 023530) used
36
37 732 here. Of note for circadian researchers, a *Vip-IRES-Cre* line also influences neuropeptide expression and
38
39 733 circadian function (Cheng et al., 2019; Joye et al., 2020).

40
41 734 We envision this line will be very useful for monitoring additional neuronal subpopulations in the
42
43 735 SCN in wild-type and mutant animals. Additional technical development may allow *in vivo* detection of
44
45 736 bioluminescence rhythms from neuronal populations in awake behaving mice. Approaches to optimize the
46
47 737 signal detected from brain include use of highly efficient and cell- and brain-penetrant substrates (Evans et
48
49 738 al., 2014; Iwano et al., 2018), cranial windows (Miller et al., 2014) and hairless or albino mice (Martin-
50
51 739 Burgos et al., 2020; Iwano et al., 2018). (Note, the tyrosinase mutation leading to albinism in C57BL/6J
52
53 740 mice is linked to *Dbp* on mouse chromosome 7; we have nevertheless generated recombinants and produced

1
2
3 741 albino reporters, including the kidney reporter mice in Fig. S3). These approaches may allow interrogation
4
5 742 of the SCN circuit *in vivo*, extending the elegant studies being performed with SCN slices *ex vivo*.
6
7 743 Bioluminescence rhythms can also be examined in neuronal populations outside the SCN, by using an
8
9 744 appropriate *Cre* driver and/or viral delivery of *Cre* recombinase.

11 745 *Cre*-mediated recombination of the *Dbp^{Kl}* allele in liver enabled us to perform continuous, *in vivo*
12
13 746 bioluminescence monitoring of liver in freely moving mice. These studies demonstrate transient
14
15 747 misalignment between the liver oscillator and SCN-regulated behavioral rhythms. Our design is
16
17 748 complementary to that used by Saini et al. (2013), who continuously monitored reporter gene
18
19 749 bioluminescence as hepatic rhythms were shifted by an inverted feeding regimen.

22 750 Repeated misalignment among oscillators is thought to contribute to adverse metabolic and health
23
24 751 consequences of chronic circadian disruption (for reviews, see Arble et al., 2015; Evans and Davidson,
25
26 752 2013; Roenneberg and Merrow, 2016; Patke et al., 2020; West & Bechtold, 2015). Up until now, technical
27
28 753 and practical limitations have restricted our ability to monitor the behavior of circadian rhythms in different
29
30 754 peripheral tissues during and following environmental disruption of circadian homeostasis. Our *Cre*-
31
32 755 conditional reporter line and the approaches described recently (Martin-Burgos et al., 2022; Tam et al.,
33
34 756 2021), and extended here for longitudinal and tissue-specific assessment of bioluminescence rhythms *in*
35
36 757 *vivo* will allow characterization of misalignment and recovery after a variety of circadian-disruptive lighting
37
38 758 and food availability paradigms. These approaches will allow more extensive examination of the
39
40 759 consequences of repeated misalignment of peripheral clocks.

43 760 The data in Figure 6 show clear misalignment between the rhythms in locomotor activity and
44
45 761 hepatic bioluminescence. Rather remarkably, the average phase of peak bioluminescence did not shift at
46
47 762 all for 3-4 days after the shift of the lighting cycle. This is consistent with previous work by others: even
48
49 763 with a more robust signal that directly impacts peripheral oscillators (reversal of the time of food
50
51 764 availability), shifting of the liver clock occurs slowly (Damiola et al., 2001; Saini et al., 2013). We did not
52
53 765 track food intake in this experiment, so do not know the rate at which the food intake pattern was reset
54
55 766 following the shift of the lighting cycle. The timing of food intake is typically controlled by the SCN,

JBR 21-117.R1

1
2
3 767 however, and thus would likely track locomotor activity. The food intake and locomotor activity rhythms
4
5 768 shift to the new phase more rapidly than the hepatic oscillator, resulting in misalignment.
6

7 769 Previous studies have shown misalignment between central and peripheral clocks induced by
8
9 770 altering the time of food access to daytime, by assessing oscillator phase at various time-points after a phase
10
11 771 shift of the lighting cycle, or by exposure to non-24hr light-dark schedules. The vast majority of these
12
13 772 studies monitored bioluminescence rhythms *ex vivo* or assessed transcript levels following tissue collection
14
15 773 at various times after a shift (Balsalobre et al., 2000; Damiola et al., 2000; Davidson et al., 2008; Davidson
16
17 774 et al., 2009; Nakamura et al., 2005; Nicholls et al., 2019; Pezuk et al., 2012; Sellix et al., 2012; Stokkan et
18
19 775 al., 2001; Yamanaka et al., 2008). Notably, *ex vivo* bioluminescence rhythm timing may be affected by
20
21 776 prior lighting conditions (Noguchi et al., 2020; Leise et al., 2020; Tahara et al., 2012). Few studies have
22
23 777 followed bioluminescence rhythms *in vivo* over time after a light-induced phase shift or after a food
24
25 778 manipulation that phase-shifts peripheral oscillators (but see Saini et al., 2013; van der Vinne et al., 2020).
26
27 779 Our current data leverage the ability to non-invasively monitor rhythmicity from a single peripheral
28
29 780 oscillator in individual animals over many days to show the time course of internal misalignment and
30
31 781 recovery after a phase shift. Other studies with minimally invasive monitoring of bioluminescence rhythms
32
33 782 have relied upon viral introduction of the reporter into liver, and thus cannot easily be extended to other
34
35 783 tissues (Saini et al., 2013; Sinturel et al., 2021). Notably, the viral reporter appears not strictly limited to
36
37 784 liver in this model (see Saini et al. 2013, their Fig S2). Moreover, efficient expression of virally delivered
38
39 785 reporter constructs is limited by the promoter size and specificity, so the level and anatomical pattern of
40
41 786 expression often do not match that of the gene whose promoter was used. Future studies of additional tissues
42
43 787 in *Cre*-conditional reporter mice will enable elucidation of how other tissues within the hierarchical, multi-
44
45 788 oscillatory circadian system respond to disruptive stimuli. Several studies suggest that organs differ in their
46
47 789 response to resetting stimuli. For example, the *Dbp* mRNA rhythm in liver is more fully reset than the
48
49 790 rhythm in heart and kidneys 3 days after restricting food availability to daytime (Damiola et al., 2000), and
50
51 791 several studies indicate the SCN (and the locomotor rhythms it regulates) resets more rapidly than
52
53 792 peripheral tissues (Davidson et al., 2008; Davidson et al., 2009; Damiola et al., 2000; Hamada et al., 2016;
54
55
56
57
58
59
60

1
2
3 793 Saini et al., 2013; Sellix et al., 2012; van der Vinne et al., 2020; Yamanaka et al., 2008; Yamazaki et al.,
4
5 794 2000; see Nicholls et al., 2019 for review).

7 795 A recent study used a feeding device similar to the one used here (Acosta-Rodriguez et al, 2017)
8
9 796 to recapitulate ‘naturalistic’ food intake patterns in mice with restricted food access (Xie et al., 2020). In
10
11 797 this study, the food restriction was not the severe ‘all or none’ patterns typically used in studies with time-
12
13 798 restricted access to food. The authors found that peripheral oscillators of *Per2^{Luciferase}* mice were not
14
15 799 effectively entrained by restricted feeding using the imposed ‘natural’ feeding patterns (Xie et al., 2020).
16
17 800 Similarly, our study (shown in Figure 7) revealed that daytime restricted food access produced a smaller
18
19 801 and more variable phase shift of the hepatic circadian clock (as indicated by the initial time-of-peak of
20
21 802 *Dbp*-driven bioluminescence) than expected based on published results using presence / absence food
22
23 803 availability cycles (Damiola et al., 2000; Hara et al., 2001; Saini et al., 2013; Stokkan et al., 2001).

26 804 Both day-to-day variation in phase of peak bioluminescence within animals as well as variation in peak
27
28 805 phase between animals is larger in the day-fed mice than in the night-fed and *ad lib* groups. These latter
29
30 806 two groups did not need to change the time of food intake greatly, while the daytime-fed group was eating
31
32 807 at an abnormal phase. Our imposing temporal restriction on feeding for only 10 days before release to DD
33
34 808 and *ad lib* feeding may not have been sufficient to synchronize liver clocks to a new phase, as suggested
35
36 809 by the partial reversal of the phase of hepatic bioluminescence. In addition, food intake patterns derived
37
38 810 from presence/absence cycles of food appear much more effective at synchronizing the liver than more
39
40 811 naturalistic food intake patterns (our data and Xie et al., 2020 compared with, for example, Saini et al.,
41
42 812 2013 and Damiola et al., 2001). The night-fed and *ad lib* groups have relatively more intense,
43
44 813 consolidated feeding in the early part of the night, which may provide a stronger stimulus to peripheral
45
46 814 oscillators, including liver. Food access for 12 hours during the daytime may be less concentrated and
47
48 815 more variable in time, providing a less effective synchronizing cue to peripheral oscillators. This may
49
50 816 lead to higher levels of within-organ desynchrony among cells and thus lower-amplitude rhythmicity,
51
52 817 secondarily leading to greater variability in determining the time of peak bioluminescence on subsequent
53
54 818 days. We also cannot rule out the possibility that the time of food intake differed between individuals and

JBR 21-117.R1

1
2
3 819 between the groups, even during *ad lib* feeding, and this could influence hepatic rhythms. Future studies
4
5 820 using a shorter duration of food access per day and monitoring bioluminescence rhythms both during the
6
7 821 acclimation to daytime feeding as well as during release to *ad lib* conditions, coupled with monitoring
8
9 822 food intake patterns throughout the study, should allow more dynamic assessment of the entrainment and
10
11 823 subsequent free-running rhythms of peripheral oscillators *in vivo*. In addition, use of a variety of different
12
13 824 *Cre* drivers will allow assessment of whether different peripheral organs respond similarly to food
14
15 825 restriction paradigms. In addition, tissue-specific reporter models will be very useful in assessing how
16
17 826 more naturalistic food ingestion paradigms influence peripheral circadian clocks in several tissues.

18
19
20 827 In summary, we have demonstrated the utility of a new, *Cre*-conditional reporter mouse that
21
22 828 enables tissue-specific monitoring of circadian molecular rhythms *in vivo* and *ex vivo*. This reporter mouse
23
24 829 provides a major advance in our capabilities for monitoring rhythms in a variety of tissues under normal
25
26 830 and disruptive conditions, which is a key step in the identification of mechanisms underlying the adverse
27
28 831 consequences of circadian disruption inherent to life in modern 24/7 societies.
29
30
31
32
33
34
35
36
37
38
39
40
41
42
43
44
45
46
47
48
49
50
51
52
53
54
55
56
57
58
59
60

1
2
3 833 **Acknowledgments**
4

5 834 We thank Christopher Lambert and Jamie Black for technical assistance, and Steven A. Brown
6
7 835 (University of Zurich) for discussions during the development of this project. UMass Chan Medical School
8
9 836 core facilities (Mutagenesis Core, Mouse Modeling Core, and Small Animal Imaging Core) are gratefully
10
11 837 acknowledged.
12

13 838 Research reported in this publication was supported by the National Institute for Neurological
14
15 839 Diseases and Stroke and the National Institute of General Medical Sciences of the National Institutes of
16
17 840 Health under award numbers R21NS103180 (DRW), SC1GM112567 (AJD), and NIGMS R15GM126545
18
19 841 (MEH), the Hartmann Müller Stiftung (RD), MRC MC_PC_15070 (RD) and BSN (RD and LAG). CBS
20
21 842 was a participant in the UMass Chan Medical School Initiative for Maximizing Student Development,
22
23 843 supported by NIH grant R25GM113686. The funders had no role in study design, data collection and
24
25 844 analysis, decision to publish, or preparation of the manuscript. The content is solely the responsibility of
26
27 845 the authors and does not necessarily represent the official views of the National Institutes of Health or the
28
29 846 other funding agencies.
30
31

32 847

33
34
35 848 **Author Contributions**

36 849 R.D and D.R.W. conceived the project
37
38 850 C.B.S., V.v.d.V., E.M., M.H.B., A.J.D., M.E.H., R.D. and D.R.W. designed research
39
40 851 C.B.S., V.v.d.V., E.M., A.C.S., B.M.B., P.C.M., L.A.G., R.D., and D.R.W. performed research
41
42 852 C.B.S., V.v.d.V., E.M., T.L.L., B.M.B., M.E.H., R.D. and D.R.W. analyzed data
43
44 853 C.B.S., V.v.d.V., and D.R.W. wrote the paper
45
46 854 All authors have approved this version of the manuscript.
47
48
49
50
51
52
53
54
55
56
57
58
59
60

856 **References.**

- 857
858 Abe M, Herzog ED, Yamazaki S, Straume M, Tei H, Sakaki Y, Menaker M, and Block GD (2002)
859 Circadian rhythms in isolated brain regions. *J Neurosci* 22:350-356.
- 860
861 Acosta-Rodriguez VA, de Groot, M H M, Rijo-Ferreira F, Green CB, and Takahashi JS (2017) Mice
862 under caloric restriction self-impose a temporal restriction of food intake as revealed by an automated
feeder system. *Cell Metab* 26:267-277.e2.
- 863
864 Balsalobre A, Brown SA, Marcacci L, Tronche F, Kellendonk C, Reichardt HM, Schutz G, and Schibler
865 U (2000) Resetting of circadian time in peripheral tissues by glucocorticoid signaling. *Science*
289:2344-2347.
- 866
867 Brandes C, Plautz JD, Stanewsky R, Jamison CF, Straume M, Wood KV, Kay SA, and Hall JC (1996)
868 Novel features of *Drosophila period* transcription revealed by real-time luciferase reporting. *Neuron*
16:687-692.
- 869
870 Cesbron F, Brunner M, and Diernfellner AC (2013) Light-dependent and circadian transcription dynamics
871 *in vivo* recorded with a destabilized luciferase reporter in *Neurospora*. *PLoS One* 8:e83660.
- 872
873 Chen Z, Yoo SH, Park YS, Kim KH, Wei S, Buhr E, Ye ZY, Pan HL, and Takahashi JS (2012)
874 Identification of diverse modulators of central and peripheral circadian clocks by high-throughput
875 chemical screening. *Proc Natl Acad Sci U S A* 109:101-106.
- 876
877 Cheng AH, Fung SW, and Cheng HM (2019) Limitations of the AVP-IRES2-Cre (JAX #023530) and
878 VIP-IRES-Cre (JAX #010908) models for chronobiological investigations. *J Biol Rhythms* 34:634-
879 644.
- 880
881 Damiola F, Le Minh N, Preitner N, Kornmann B, Fleury-Olela F, and Schibler U (2000) Restricted
882 feeding uncouples circadian oscillators in peripheral tissues from the central pacemaker in the
suprachiasmatic nucleus. *Genes Dev* 14:2950-2961.
- 883
884 Davidson AJ, Castanon-Cervantes O, Leise TL, Molyneux PC, and Harrington ME (2009) Visualizing jet
lag in the mouse suprachiasmatic nucleus and peripheral circadian timing system. *Eur J Neurosci*
29:171-180.
- 885
886 Davidson AJ, Yamazaki S, Arble DM, Menaker M, and Block GD (2008) Resetting of central and
887 peripheral circadian oscillators in aged rats. *Neurobiol Aging* 29:471-477.
- 888
889 Destici E, Jacobs EH, Tamanini F, Loos M, van der Horst GTJ, Oklejewicz M (2013) Altered phase-
relationship between peripheral oscillators and environmental time in *Cry1* or *Cry2* deficient mouse
models for early and late chronotypes. *PLoS ONE* 8, e83802.
- 890
891 Evans JA and Davidson AJ (2013) Health consequences of circadian disruption in humans and animal
models. *Prog Mol Biol Transl Sci* 119:283-323.
- 892
893 Evans JA, Leise TL, Castanon-Cervantes O, and Davidson AJ (2013) Dynamic interactions mediated by
nonredundant signaling mechanisms couple circadian clock neurons. *Neuron* 80:973-983.
- 894
895 Evans JA, Leise TL, Castanon-Cervantes O, and Davidson AJ (2011) Intrinsic regulation of
spatiotemporal organization within the suprachiasmatic nucleus. *PLoS One* 6:e15869.
- 896
897 Evans MS, Chauréte JP, Adams ST, Reddy GR, Paley MA, Aronin N, Prescher JA, and Miller SC (2014) A
synthetic luciferin improves bioluminescence imaging in live mice. *Nat Methods* 11:393-395.

- 1
2
3 896 Fonjallaz P, Ossipow V, Wanner G, and Schibler U (1996) The two PAR leucine zipper proteins, TEF
4 897 and DBP, display similar circadian and tissue-specific expression, but have different target promoter
5 898 preferences. *EMBO J* 15:351-362.
6
7 899 Goyal V, DeVera C, Baba K, Sellers J, Chrenek MA, Iuvone PM, Tosini G (2021) Photoreceptor
8 900 degeneration in homozygous male *Per2^{luc}* mice during aging. *J Biol Rhythms* 36:137-145.
9
10 901 Hamada T, Sutherland K, Ishikawa M, Miyamoto N, Honma S, Shirato H, and Honma K (2016) *In vivo*
11 902 imaging of clock gene expression in multiple tissues of freely moving mice. *Nat Commun* 7:11705.
12
13 903 Hara R, Wan K, Wakamatsu H, Aida R, Moriya T, Akiyama M, and Shibata S (2001) Restricted feeding
14 904 entrains liver clock without participation of the suprachiasmatic nucleus. *Genes Cells* 6:269-278.
15
16 905 Harris JA, Hirokawa KE, Sorensen SA, Gu H, Mills M, Ng LL, Bohn P, Mortrud M, Ouellette B, Kidney
17 906 J, Smith KA, Dang C, Sunkin S, Bernard A, Oh SW, Madisen L, and Zeng H (2014) Anatomical
18 907 characterization of Cre driver mice for neural circuit mapping and manipulation. *Front Neural*
19 908 *Circuits* 8:76.
20
21 909 Herzog ED hermanstynne T, Smyllie NJ, Hastings MH (2017) Regulating the suprachiasmatic nucleus
22 910 (SCN) clockwork: Interplay between cell-autonomous and circuit-level mechanisms. *Cold Springs*
23 911 *Harbor Perspect Biol* 9: a027706.
24
25 912 Hirota T, Lee JW, Lewis WG, Zhang EE, Breton G, Liu X, Garcia M, Peters EC, Etchegaray JP, Traver
26 913 D, Schulz PG, Kay SA (2010) High-throughput chemical screen identified a novel potent modulator
27 914 of cellular circadian rhythms and reveals CK1 alpha as a clock regulatory kinase. *PLoS Biol* 8,
28 915 e1000559
29
30 916 Iwano S, Sugiyama M, Hama H, Watakabe A, Hasegawa N, Kuchimaru T, Tanaka KZ, Takahashi M, Ishida
31 917 Y, Hata J, Shimozono S, Namiki K, Fukano T, Kiyama M, Okano H, Kizaka-Kondoh S, McHugh TJ,
32 918 Yamamori T, Hioki H, Maki S, and Miyawaki A (2018) Single-cell bioluminescence imaging of deep
33 919 tissue in freely moving animals. *Science* 359:935-939.
34
35 920 Joye DAM, Rohr KE, Keller D, Inda T, Telega A, Pancholi H, Carmona-Alcocer V, and Evans JA (2020)
36 921 Reduced VIP expression affects circadian clock function in VIP-IRES-CRE Mice (JAX 010908). *J*
37 922 *Biol Rhythms* 35:340-352.
38
39 923 Kim JH, Lee SR, Li LH, Park HJ, Park JH, Lee KY, Kim MK, Shin BA, Choi SY. (2011) High cleavage
40 924 efficiency of a 2A peptide derived from porcine Teschovirus-1 in human cell lines, zebrafish and
41 925 mice. *PLoS ONE* 6, e18556
42
43 926 Kondo T, Strayer CA, Kulkarni RD, Taylor W, Ishiura M, Golden SS, and Johnson CH (1993) Circadian
44 927 rhythms in prokaryotes: luciferase as a reporter of circadian gene expression in cyanobacteria. *Proc*
45 928 *Natl Acad Sci U S A* 90:5672-5676.
46
47 929 Kuhlman SJ, Quintero JE, McMahon DG (2000) GFP fluorescence reports *Period 1* circadian gene
48 930 regulation in the mammalian biological clock. *NeuroReport* 11:1479-1482.
49
50 931 Kwon PK, Kim H-M, Kim SW, Kang B, Yi H, Ku H-O, Roh T-Y, Kim K-T (2019) The poly(C) motif in
51 932 the proximal promoter region of D site-binding protein gene (*Dbp*) drives its high-amplitude
52 933 oscillation. *Mol Cell Biol* 39:e00101-19
53
54 934 Kwon PK, Lee K-H, Kim J-h, Tae S, Ham S, Jeong Y-H, Kim SW, Kang B, Kim H-M, Choi J-H, Yi H,
55 935 Ku H-O, Roh T-Y, Lim C, Kim K-T (2020) hnRNP K supports high-amplitude D site-binding protein
56 936 mRNA (*Dbp* mRNA) oscillation to sustain circadian rhythms. *Mol Cell Biol* 40:e00537-19.

JBR 21-117.R1

- 1
2
3 937
4 938
5
6 939 Lee IT, Chang AS, Manandhar M, Shan Y, Fan J, Izumo M, Ikeda Y, Motoike T, Dixon S, Seinfeld JE,
7 940 Takahashi JS, and Yanagisawa M (2015) Neuromedin S-producing neurons act as essential
8 941 pacemakers in the suprachiasmatic nucleus to couple clock neurons and dictate circadian rhythms.
9 942 Neuron 85:1086-1102.
- 10
11 943 Leise TL (2017) Analysis of nonstationary time series for biological rhythms research. J Biol Rhythms
12 944 32:187-194.
- 13
14 945 Leise TL, Goldberg A, Michael J, Montoya G, Solow S, Molyneux P, Vetrivelan R, and Harrington ME
15 946 (2020) Recurring circadian disruption alters circadian clock sensitivity to resetting. Eur J Neurosci
16 947 51:2343-2354.
- 17
18 948 Leise TL and Harrington ME (2011) Wavelet-based time series analysis of circadian rhythms. J Biol
19 949 Rhythms 26:454-463.
- 20
21 950 Leise TL, Harrington ME, Molyneux PC, Song I, Queenan H, Zimmerman E, Lall GS, and Biello SM
22 951 (2013) Voluntary exercise can strengthen the circadian system in aged mice. Age (Dordr) 35:2137-
23 952 2152.
- 24
25 953 Logan M, Martin JF, Nagy A, Lobe C, Olson EN, and Tabin CJ (2002) Expression of Cre recombinase in
26 954 the developing mouse limb bud driven by a Prxl enhancer. Genesis 33:77-80.
- 27
28 955 Lopez-Molina L, Conquet F, Dubois-Dauphin M, and Schibler U (1997) The DBP gene is expressed
29 956 according to a circadian rhythm in the suprachiasmatic nucleus and influences circadian behavior.
30 957 EMBO J 16:6762-6771.
- 31
32 958 Martin-Burgos B, Wang W, William I, Tir S, Mohammad I, Javed R, Smith S, Cui Y, Smith CB, van
33 959 der Vinne V, Molyneux PC, Miller SC, Weaver DR, Leise TL, Harrington ME (2020) Methods for
34 960 detecting PER2::LUCIFERASE bioluminescence rhythms in freely moving mice. *BioRxiv*
35 961 <https://doi.org/10.1038/s41467-017-00462-2>. *Journal of Biological Rhythms*, in press 2022.
- 36
37 962 Maywood ES, Drynan L, Chesham JE, Edwards MD, Dardente H, Fustin JM, Hazlerigg DG, O'Neill JS,
38 963 Codner GF, Smyllie NJ, Brancaccio M, and Hastings MH (2013) Analysis of core circadian feedback
39 964 loop in suprachiasmatic nucleus of *mCry1-luc* transgenic reporter mouse. Proc Natl Acad Sci U S A
40 965 110:9547-9552.
- 41
42 966 Mei L, Fan Y, Lv X, Welsh DK, Zhan C, and Zhang EE (2018) Long-term in vivo recording of circadian
43 967 rhythms in brains of freely moving mice. Proc Natl Acad Sci U S A 115:4276-4281.
- 44
45 968 Mieda M, Okamoto H, and Sakurai T (2016) Manipulating the cellular circadian period of arginine
46 969 vasopressin neurons alters the behavioral circadian period. Curr Biol 26:2535-2542.
- 47
48 970 Mieda M, Ono D, Hasegawa E, Okamoto H, Honma K, Honma S, and Sakurai T (2015) Cellular clocks
49 971 in AVP neurons of the SCN are critical for interneuronal coupling regulating circadian behavior
50 972 rhythm. Neuron 85:1103-1116.
- 51
52 973 Millar AJ, Short SR, Chua NH, and Kay SA (1992) A novel circadian phenotype based on firefly
53 974 luciferase expression in transgenic plants. Plant Cell 4:1075-1087.
- 54
55 975 Millar AJ, Carre IA, Strayer CA, Chua NH, Kay SA (1995). Circadian clock mutants in Arabidopsis
56 976 identified by luciferase imaging. Science 267:1161-1163.

- 1
2
3 977 Miller JE, Granados-Fuentes D, Wang T, Marpegan L, Holy TE, and Herzog ED (2014) Vasoactive
4 978 intestinal polypeptide mediates circadian rhythms in mammalian olfactory bulb and olfaction. J
5 979 Neurosci 34:6040-6046.
6
7 980 Mohawk JA, Green CB, and Takahashi JS (2012) Central and peripheral circadian clocks in mammals.
8 981 Annu Rev Neurosci 35:445-462.
9
10 982 Morgan LW, Greene AV, and Bell-Pedersen D (2003) Circadian and light-induced expression of
11 983 luciferase in *Neurospora crassa*. Fungal Genet Biol 38:327-332.
12
13 984 Muñoz-Guzmán F, Caballero V, and Larrondo LF (2021) A global search for novel transcription factors
14 985 impacting the *Neurospora crassa* circadian clock. G3 (Bethesda). DOI: 10.1093/g3journal/jkab100
15
16 986 Nagano M, Adachi A, Nakahama K, Nakamura T, Tamada M, Meyer-Bernstein E, Sehgal A, and
17 987 Shigeyoshi Y (2003) An abrupt shift in the day/night cycle causes desynchrony in the mammalian
18 988 circadian center. J Neurosci 23:6141-6151.
19
20 989 Nagoshi E, Saini C, Bauer C, Laroche T, Naef F, and Schibler U (2004) Circadian gene expression in
21 990 individual fibroblasts: cell-autonomous and self-sustained oscillators pass time to daughter cells. Cell
22 991 119:693-705.
23
24 992 Nakamura W, Yamazaki S, Takasu NN, Mishima K, and Block GD (2005) Differential response of
25 993 *Period 1* expression within the suprachiasmatic nucleus. J Neurosci 25:5481-5487.
26
27 994 Nakamura W, Yamazaki S, Nakamura TJ, Shirakawa T, Block GD, and Takumi T (2008) *In vivo*
28 995 monitoring of circadian timing in freely moving mice. Curr Biol 18:381-385.
29
30 996 Nicholls SK, Casiraghi LP, Wang W, Weber ET, and Harrington ME (2019) Evidence for internal
31 997 desynchrony caused by circadian clock resetting. Yale J Biol Med 92:259-270.
32
33 998 Noguchi T, Harrison EM, Sun J, May D, Ng A, Welsh DK, and Gorman MR (2020) Circadian rhythm
34 999 bifurcation induces flexible phase resetting by reducing circadian amplitude. Eur J Neurosci 51:2329-
35 1000 2342.
36
37 1001 Ono D, Honma K, and Honma S (2015a) Circadian and ultradian rhythms of clock gene expression in the
38 1002 suprachiasmatic nucleus of freely moving mice. Sci Rep 5:12310.
39
40 1003 Patke A, Young MW, and Axelrod S (2020) Molecular mechanisms and physiological importance of
41 1004 circadian rhythms. Nat Rev Mol Cell Biol 21:67-84.
42
43 1005 Pezuk P, Mohawk JA, Wang LA, and Menaker M (2012) Glucocorticoids as entraining signals for
44 1006 peripheral circadian oscillators. Endocrinology 153:4775-4783.
45
46 1007 Postic C, Shiota M, Niswender KD, Jetton TL, Chen Y, Moates JM, Shelton KD, Lindner J, Cherrington
47 1008 AD, and Magnuson MA (1999) Dual roles for glucokinase in glucose homeostasis as determined by
48 1009 liver and pancreatic beta cell-specific gene knock-outs using Cre recombinase. J Biol Chem 274:305-
49 1010 315.
50
51 1011 Poulsen RC, Warman GR, Sleight J, Ludin NM, and Cheeseman JF (2018) How does general anaesthesia
52 1012 affect the circadian clock? Sleep Med Rev 37:35-44.
53
54 1013 Punia S, Rumery KK, Yu EA, Lambert CM, Notkins AL, and Weaver DR (2012) Disruption of gene
55 1014 expression rhythms in mice lacking secretory vesicle proteins IA-2 and IA-2 β . Am J Physiol
56 1015 Endocrinol Metab 303:762.
57
58
59
60

JBR 21-117.R1

- 1
2
3 1016 Ralph MR, Shi SQ, Johnson CH, Houdek P, Shrestha TC, Crosby P, O'Neill JS, Sladek M, Stinchcombe
4 1017 AR, and Sumova A (2021) Targeted modification of the *Per2* clock gene alters circadian function in
5 1018 *mPer2^{luciferase} (mPer2^{Luc})* mice. *PLoS Comput Biol* 17:e1008987.
- 7 1019 Reddy AB, Field MD, Maywood ES, and Hastings MH (2002) Differential resynchronization of circadian
8 1020 clock gene expression within the suprachiasmatic nuclei of mice subjected to experimental jet lag. *J*
9 1021 *Neurosci* 22:7326-7330.
- 11 1022 Ripperger JA and Schibler U (2006) Rhythmic CLOCK-BMAL1 binding to multiple E-box motifs drives
12 1023 circadian Dbp transcription and chromatin transitions. *Nat Genet* 38:369-374.
- 14 1024 Ripperger JA, Shearman LP, Reppert SM, Schibler U (2000) CLOCK, an essential pacemaker
15 1025 component, controls expression of the circadian transcription factor DBP. *Genes Dev* 14:679-689.
- 17 1026 Roenneberg T and Merrow M (2016) The Circadian Clock and Human Health. *Curr Biol* 26:432.
- 19 1027 Saini C, Liani A, Curie T, Gos P, Kreppel F, Emmenegger Y, Bonacina L, Wolf JP, Poget YA, Franken
20 1028 P, and Schibler U (2013) Real-time recording of circadian liver gene expression in freely moving
21 1029 mice reveals the phase-setting behavior of hepatocyte clocks. *Genes Dev* 27:1526-1536.
- 23 1030 Sawai Y, Okamoto T, Muranaka Y, Nakamura R, Matsumura R, Node K, and Akashi M (2019) *In vivo*
24 1031 evaluation of the effect of lithium on peripheral circadian clocks by real-time monitoring of clock gene
25 1032 expression in near-freely moving mice. *Sci Rep* 9:10909-3.
- 27 1033 Sellix MT, Evans JA, Leise TL, Castanon-Cervantes O, Hill DD, DeLisser P, Block GD, Menaker M, and
28 1034 Davidson AJ (2012) Aging differentially affects the re-entrainment response of central and peripheral
29 1035 circadian oscillators. *J Neurosci* 32:16193-16202.
- 31 1036 Shan Y, Abel JH, Li Y, Izumo M, Cox KH, Jeong B, Yoo SH, Olson DP, Doyle FJ, and Takahashi JS
32 1037 (2020) Dual-color single-cell imaging of the Suprachiasmatic Nucleus reveals a circadian role in
33 1038 network synchrony. *Neuron* 108:164-179.e7
- 35 1039 Shao X; Somlo S; Igarashi P (2002) Epithelial-specific Cre/lox recombination in the developing kidney
36 1040 and genitourinary tract. *J Am Soc Nephrol* 13: 1837-1846.
- 38 1041 Sinturel F, Gos P, Petrenko V, Hagedorn C, Kreppel F, Storch KF, Knutti D, Liani A, Weitz C,
39 1042 Emmenegger Y, Franken P, Bonacina L, Dibner C, and Schibler U (2021) Circadian hepatocyte
40 1043 clocks keep synchrony in the absence of a master pacemaker in the suprachiasmatic nucleus or other
41 1044 extrahepatic clocks. *Genes Dev* 35:329-334.
- 43 1045 Smyllie NJ, Pilorz V, Boyd J, Meng QJ, Saer B, Chesham JE, Maywood ES, Krogager TP, Spiller DG,
44 1046 Boot-Handford R, White MR, Hastings MH, Loudon AS (2016) Visualizing and quantifying
45 1047 intracellular behavior and abundance of the core circadian clock protein PERIOD2. *Curr Biol*
46 1048 26:1880-1886.
- 48 1050 Stanewsky R, Kaneko M, Emery P, Beretta B, Wager-Smith K, Kay SA, Rosbash M, and Hall JC (1998)
49 1051 The *cry^b* mutation identifies cryptochrome as a circadian photoreceptor in *Drosophila*. *Cell* 95:681-
50 1052 692.
- 52 1053 Stokkan KA, Yamazaki S, Tei H, Sakaki Y, and Menaker M (2001) Entrainment of the circadian clock in
53 1054 the liver by feeding. *Science* 291:490-493.

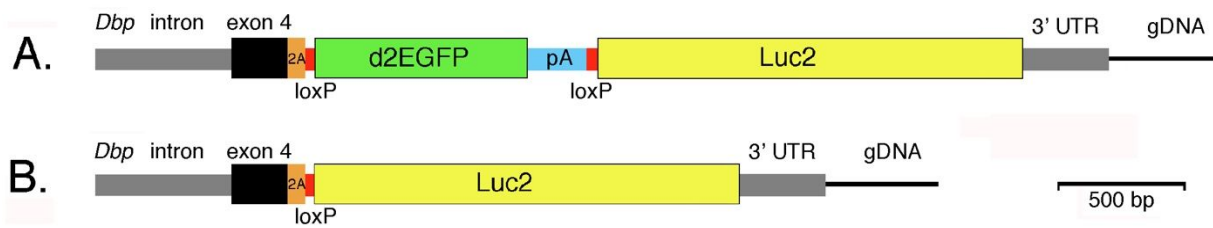
- 1
2
3 1055 Stratmann M, Suter DM, Molina N, Naef F, and Schibler U (2012) Circadian *Dbp* transcription relies on
4 1056 highly dynamic BMAL1-CLOCK interaction with E boxes and requires the proteasome. *Mol Cell*
5 1057 48:277-287.
6
7 1058 Tahara Y, Kuroda H, Saito K, Nakajima Y, Kubo Y, Ohnishi N, Seo Y, Otsuka M, Fuse Y, Ohura Y,
8 1059 Komatsu T, Moriya Y, Okada S, Furutani N, Hirao A, Horikawa K, Kudo T, and Shibata S (2012) *In*
9 1060 *vivo* monitoring of peripheral circadian clocks in the mouse. *Curr Biol* 22:1029-1034.
10
11 1061 Tam SKE, Brown LA, Wilson TS, Tir S, Fisk AS, Potheary CA, van der Vinne V, Foster RG,
12 1062 Vyazovskiy VV, Bannerman DM, Harrington ME, Peirson SN (2021) Dim light in the evening
13 1063 causes coordinated realignment of circadian rhythms, sleep, and short-term memory. *Proc Natl Acad*
14 1064 *Sci* 118:e2101591118. doi: 10.1073/pnas.2101591118.
15
16 1065 van der Vinne V, Martin Burgos B, Harrington ME, and Weaver DR (2020) Deconstructing circadian
17 1066 disruption: Assessing the contribution of reduced peripheral oscillator amplitude on obesity and
18 1067 glucose intolerance in mice. *J Pineal Res* 69:e12654.
19
20 1068 van der Vinne V, Swoap SJ, Vajtay TJ, and Weaver DR (2018) Desynchrony between brain and
21 1069 peripheral clocks caused by CK1 δ/ϵ disruption in GABA neurons does not lead to adverse metabolic
22 1070 outcomes. *Proc Natl Acad Sci U S A* 115:E2437-E2446.
23
24 1071 Weaver DR, van der Vinne V, Giannaris EL, Vajtay TJ, Holloway KL, and Anaclet C (2018)
25 1072 Functionally complete excision of conditional alleles in the mouse suprachiasmatic nucleus by *Vgat-*
26 1073 *IRE5-Cre*. *J Biol Rhythms* 33:179-191.
27
28 1074 Weger M, Weger BD, Diotel N, Rastegar S, Hirota T, Kay SA, Strahle U, and Dickmeis T (2013) Real-
29 1075 time *in vivo* monitoring of circadian E-box enhancer activity: a robust and sensitive zebrafish reporter
30 1076 line for developmental, chemical and neural biology of the circadian clock. *Dev Biol* 380:259-273.
31
32 1077 Welsh DK, Yoo SH, Liu AC, Takahashi JS, Kay SA (2004) Bioluminescence imaging of individual
33 1078 fibroblasts reveals persistent, independently phased circadian rhythms of clock gene expression. *Curr*
34 1079 *Biol* 14:2289-2295.
35
36 1080 West AC and Bechtold DA (2015) The cost of circadian desynchrony: Evidence, insights and open
37 1081 questions. *Bioessays* 37:777-788.
38
39 1082 Xie X, Kukino A, Calcagno HE, Berman AM, Garner JP, and Butler MP (2020) Natural food intake
40 1083 patterns have little synchronizing effect on peripheral circadian clocks. *BMC Biol* 18:160-7.
41
42 1084 Yagita K, Okamura H (2000) Forskolin induces circadian gene expression of rPer1, rPer2 and dbp in
43 1085 mammalian rat-1 fibroblasts. *FEBS Lett* 465:79-82.
44
45 1086 Yamaguchi S, Kobayashi M, Mitsui S, Ishida Y, van der Horst, G. T., Suzuki M, Shibata S, and Okamura
46 1087 H (2001) View of a mouse clock gene ticking. *Nature* 409:684.
47
48 1088 Yamaguchi Y, Suzuki T, Mizoro Y, Kori H, Okada K, Chen Y, Fustin JM, Yamazaki F, Mizuguchi N,
49 1089 Zhang J, Dong X, Tsujimoto G, Okuno Y, Doi M, and Okamura H (2013) Mice genetically deficient
50 1090 in vasopressin V1a and V1b receptors are resistant to jet lag. *Science* 342:85-90.
51
52 1091 Yamaguchi Y, Okada K, Mizuno T, Ota T, Yamada H, Doi M, Kobayashi M, Tei H, Shigeyoshi Y,
53 1092 Okamura H (2016). Real-time recording of circadian *Per1* and *Per2* expression in the
54 1093 suprachiasmatic nucleus of freely moving rats. *J Biol Rhythms* 31:108-111.
55
56
57
58
59
60

JBR 21-117.R1

- 1
2
3 1094 Yamanaka Y, Honma S, and Honma K (2008) Scheduled exposures to a novel environment with a
4 1095 running-wheel differentially accelerate re-entrainment of mice peripheral clocks to new light-dark
5 1096 cycles. *Genes Cells* 13:497-507.
- 7 1097 Yamazaki S and Takahashi JS (2005) Real-time luminescence reporting of circadian gene expression in
8 1098 mammals. *Methods Enzymol* 393:288-301.
- 10 1099 Yamazaki S, Numano R, Abe M, Hida A, Takahashi R, Ueda M, Block GD, Sakaki Y, Menaker M, and
11 1100 Tei H (2000) Resetting central and peripheral circadian oscillators in transgenic rats. *Science*
12 1101 288:682-685.
- 14 1102 Yan L, Miyake S, Okamura H (2000) Distribution and circadian expression of *dbp* in SCN and extra-SCN
15 1103 areas in the mouse brain. *J Neurosci Res* 59:291-295.
- 17 1104 Yang N, Smyllie NJ, Morris H, Gonçalves CF, Dudek M, Pathirana DRJ, Chesham JE, Adamson A,
18 1105 Spiller DG, Zindy E, Bagnall J, Humphreys N, Hoyland J, Loudon ASI, Hastings MH, Meng QJ
19 1106 (2020) Quantitative live imaging of Venus::BMAL1 in a mouse model reveals complex dynamics of
20 1107 the master circadian clock regulator. *PLoS Genet* 16: e1008729. doi: 10.1371/journal.pgen.1008729.
- 22 1108 Yoo SH, Ko CH, Lowrey PL, Buhr ED, Song EJ, Chang S, Yoo OJ, Yamazaki S, Lee C, and Takahashi
23 1109 JS (2005) A noncanonical E-box enhancer drives mouse *Period2* circadian oscillations *in vivo*. *Proc*
24 1110 *Natl Acad Sci U S A* 102:2608-2613.
- 26 1111 Yoo SH, Yamazaki S, Lowrey PL, Shimomura K, Ko CH, Buhr ED, Siepk SM, Hong HK, Oh WJ, Yoo
27 1112 OJ, Menaker M, and Takahashi JS (2004) PERIOD2::LUCIFERASE real-time reporting of circadian
28 1113 dynamics reveals persistent circadian oscillations in mouse peripheral tissues. *Proc Natl Acad Sci U S*
29 1114 *A* 101:5339-5346.
- 31 1115 Yoo SH, Kojima S, Shimomura K, Koike N, Buhr ED, Furukawa T, Ko CH, Gloston G, Ayoub C,
32 1116 Nohara K, Reyes BA, Tsuchiya Y, Yoo OJ, Yagita K, Lee C, Chen Z, Yamazaki S, Green CB, and
33 1117 Takahashi JS (2017) *Period2* 3'-UTR and microRNA-24 regulate circadian rhythms by repressing
34 1118 PERIOD2 protein accumulation. *Proc Natl Acad Sci U S A* 114:E8855-E8864.
- 36 1119 Zhang EE, Liu AC, Hirota T, miraglia LJ, Welch G, Pongsawakul PY, liu X, Atwood A, Huss JW 3rd,
37 1120 Janes J, Su AI, Hogenesch JB, Kay SA (2009) A genome-wide RNAi screen for modulators of the
38 1121 circadian clock in human cells *Cell* 139: 199-210.
- 40 1122 Zhang R, Lahens NF, Ballance HI, Hughes ME, and Hogenesch JB (2014) A circadian gene expression
41 1123 atlas in mammals: implications for biology and medicine. *Proc Natl Acad Sci U S A* 111:16219-
42 1124 16224.
- 43
44
45
46
47
48
49
50
51
52
53
54
55
56
57

1125 **Figures and Tables**

1126



1127

1128 **Figure 1. Generation of a bifunctional reporter from the mouse *Dbp* locus.**

1129 **A.** The mouse *Dbp* locus was modified by CRISPR-mediated insertion of the donor construct shown. The
 1130 construct contained homology arms from the *Dbp* locus (gray and black) and inserted the reporter sequences
 1131 with a T2A-encoding sequence (orange) between DBP and the reporter. Destabilized EGFP (d2EGFP) with
 1132 a bovine growth hormone polyadenylation site (PA) was flanked by *loxP* sites (red). Downstream of *GFP*
 1133 is a luciferase (*Luc2*) reporter gene. Without recombination *Dbp* and *GFP* are expressed as a single
 1134 transcript from the conditional (*Dbp^{KI}* allele).

1135 **B.** With *Cre*-mediated recombination, GFP-encoding sequences are excised and *Dbp* and *luciferase* are
 1136 expressed as a single transcript. The T2A sequence generates separate proteins from these bifunctional
 1137 transcripts. *Cre*-mediated germline recombination led to mice expressing luciferase non-conditionally from
 1138 the *Dbp^{Luc}* allele.

1139

1140

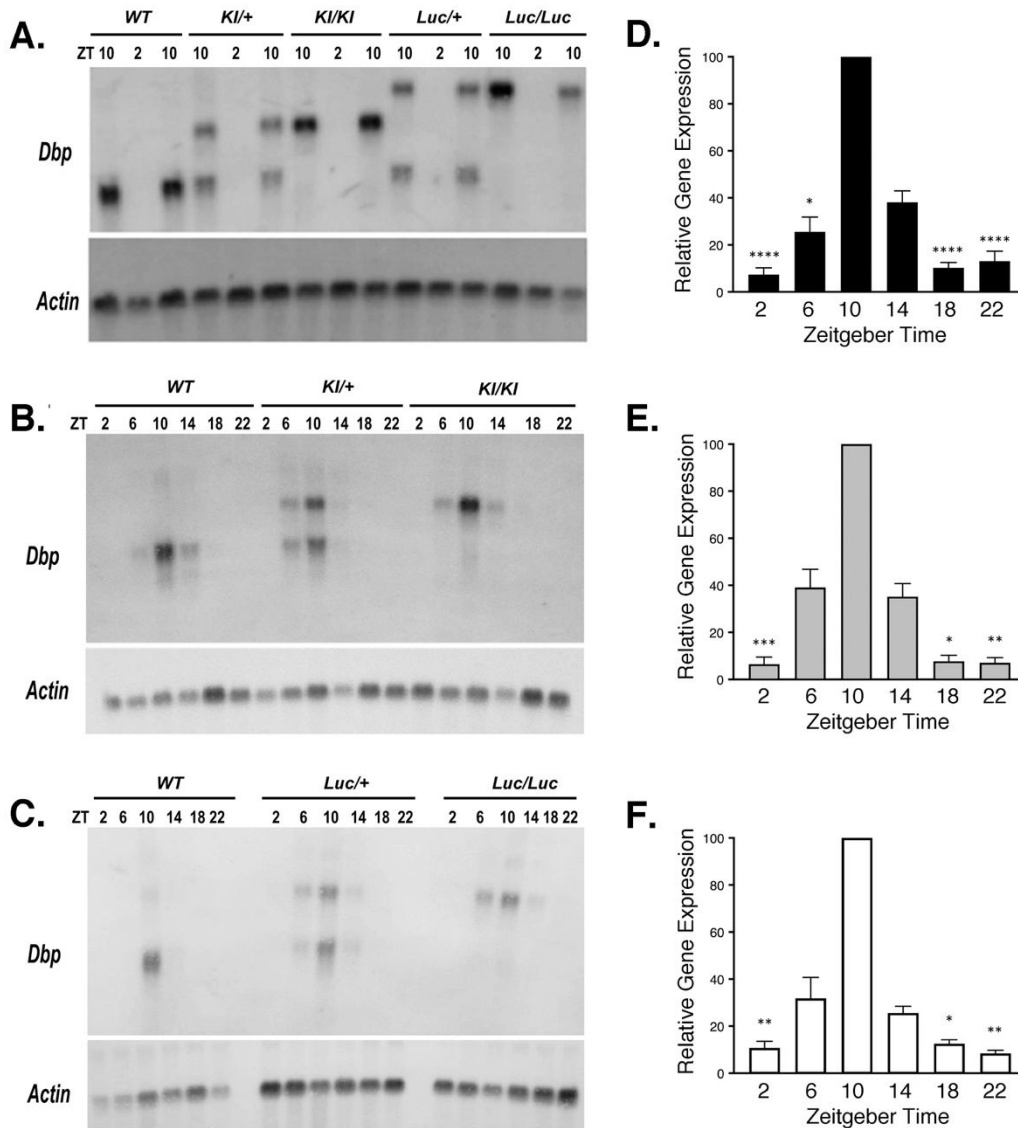


Figure 2. *Dbp* mRNA rhythms are not altered in reporter mice.

A-C. Representative Northern Blots probed to detect *Dbp* and *Actin* mRNA. **A.** From each of five genotypes, RNA samples were extracted from livers collected at ZT 2 and 10. For each genotype, there are two samples at ZT10 and one sample at ZT2 on this blot. **B.** and **C.** Representative Northern Blots of RNA samples collected from WT and reporter mouse livers at each of six Zeitgeber times (ZT).

D-F. Quantification of *Dbp* mRNA rhythms for each allele in time-series experiments (6 time-points each). Results are expressed as mean (\pm SEM) percent of the peak *Dbp/Actin* ratio, which occurred at ZT 10 on every blot. **D.** Wild-type *Dbp* transcript (n=12 sample sets). **E.** *Dbp*^{KI} transcript (n=6). **F.** *Dbp*^{Luc} transcript (n=6). For each transcript, there was a significant rhythm (Friedman's One-way ANOVA, $Q > 19$, $p < 0.002$). Asterisks indicate time-points that differed significantly from ZT10 (Dunn's test, * $p < 0.05$, ** $p < 0.01$).

1
2
3 1152 < 0.01, *** $p < 0.001$, **** $p \leq 0.0001$). Significant differences among some other time-points are not
4 1153 shown for clarity.
5
6 1154
7
8
9
10
11
12
13
14
15
16
17
18
19
20
21
22
23
24
25
26
27
28
29
30
31
32
33
34
35
36
37
38
39
40
41
42
43
44
45
46
47
48
49
50
51
52
53
54
55
56
57
58
59
60

For Peer Review

JBR 21-117.R1

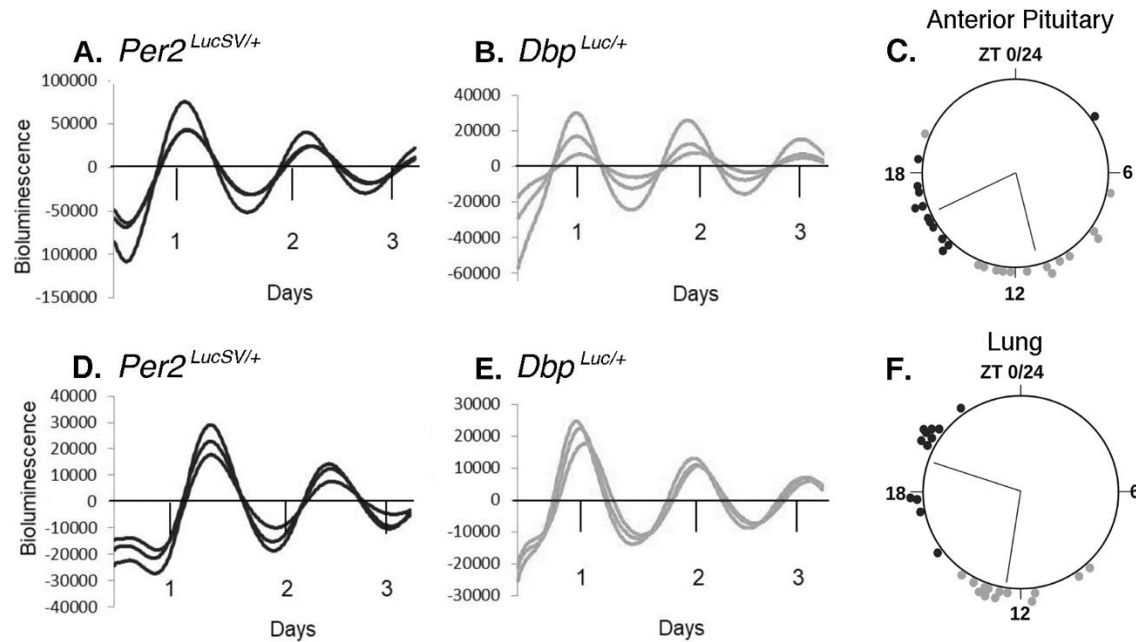
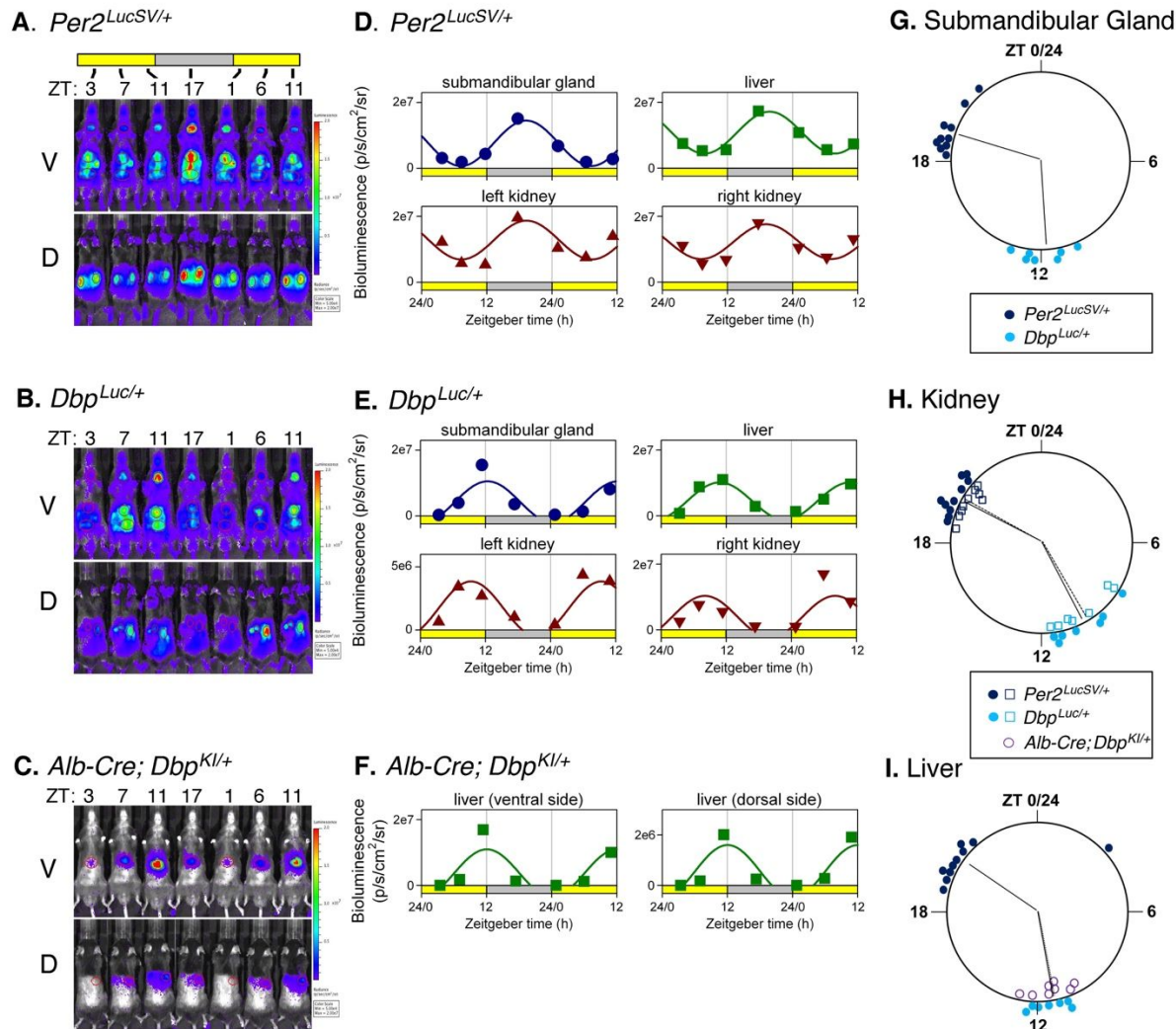


Figure 3. Ex vivo bioluminescence rhythms from *Per2*^{LucSV/+} and *Dbp*^{Luc/+} tissue explants.

A-C., Anterior Pituitary gland. D-F., Lung.

A., B., D., and E. are representative bioluminescence rhythms from triplicate tissue explants from *Per2*^{LucSV/+} (A., D.) and *Dbp*^{Luc/+} mice (B., E.). ‘Days’ refers to time in culture, not projected ZT. Values are 24-h background-subtracted and 3-h smoothed.

C., F., Time of peak bioluminescence *ex vivo*. The large circles represent a 24-h day for each organ. ZT’s refer to the lighting cycle to which the mice were exposed prior to sample collection, with ZT0-12 being the light phase. Circles at the perimeter of the large circle indicate the timing of peak bioluminescence of individual *Per2*^{LucSV/+} (black) or *Dbp*^{Luc/+} (gray) tissue explants (n=12-14 mice). Within each tissue/genotype combination, there was significant clustering of times of peak bioluminescence. Radial lines represent the mean peak time, which differed significantly between genotypes for each tissue (Watson-Williams test, $p < 0.001$).



1170
1171 **Figure 4. Bioluminescence rhythms measured *in vivo*.**

1172 A-C. Bioluminescence images captured at 4-6 hr intervals from a representative mouse of each genotype.
1173 A. *Per2^{LucSV/+}*, B. *Dbp^{Luc/+}* C. *Alb-Cre⁺; Dbp^{KI/+}*. Ventral (V) and dorsal (D) views are shown for each
1174 mouse. All images for each mouse are set to the same luminescence scale.

1175 D-F. Cosinor-fitting of bioluminescence signal over time for the animals shown in Panels A-C to determine
1176 peak time. Bioluminescence rhythms were assessed in submandibular gland, liver, and kidneys of (D.)
1177 *Per2^{LucSV/+}* and (E.) *Dbp^{Luc/+}* reporter mice, and from liver of *Alb-Cre⁺; Dbp^{KI/+}* mice (F.).

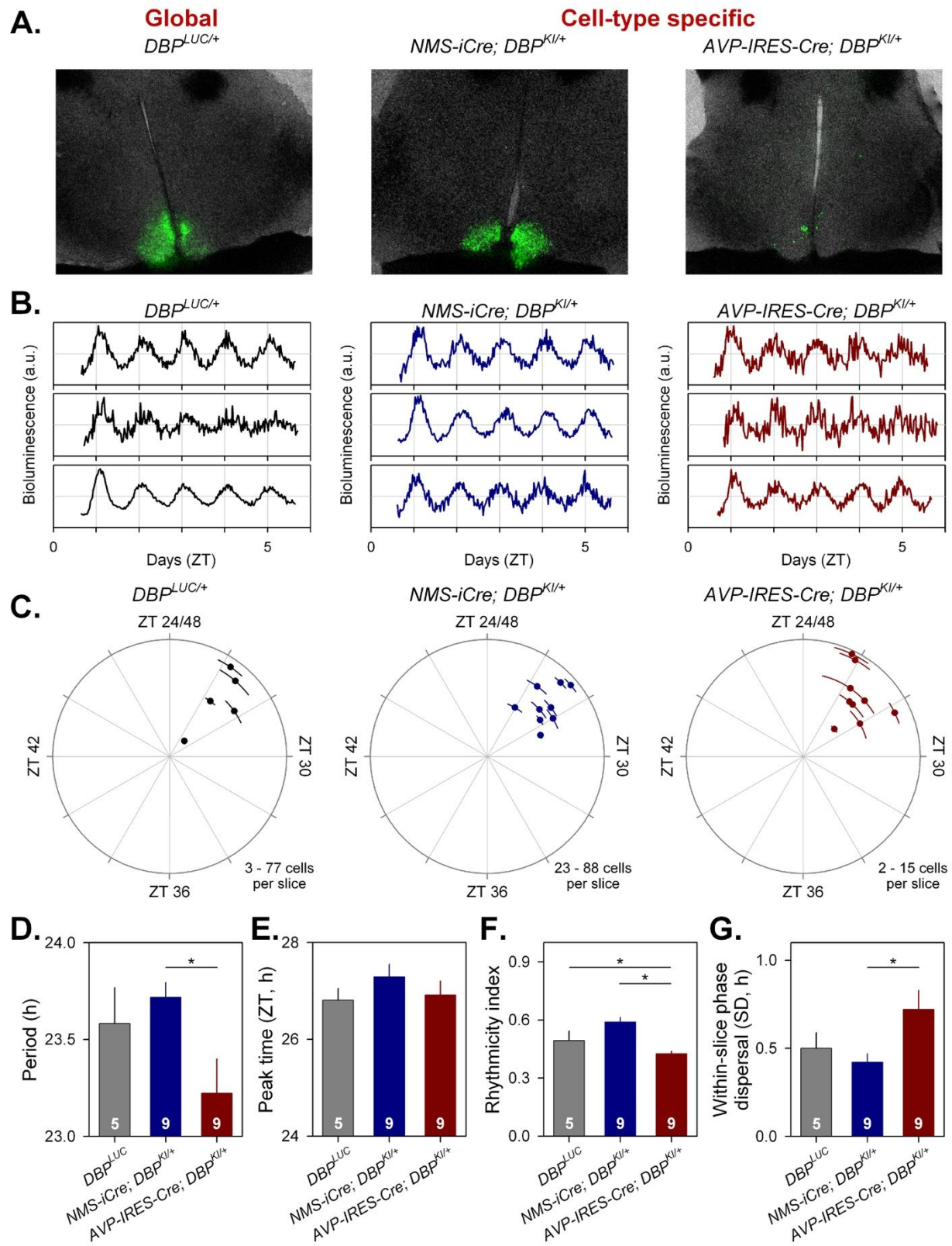
1178 G-I. Time of peak bioluminescence *in vivo*. G. Submandibular gland, H. Kidneys, and I. Liver. Data plotted
1179 as in Fig. 3. *Per2^{LucSV/+}* tissues (n=10, dark blue), *Dbp^{Luc/+}* tissues (n=7, teal). In Panel H, open squares and
1180 filled circles represent the right and left kidneys, respectively. In Panel I, purple circles represent livers
1181 from *Alb-Cre⁺; Dbp^{KI/+}* mice (n=8). Radial lines represent the mean peak time for each genotype and
1182 tissue. Radial lines from the two kidneys of a genotype are nearly overlapping. For liver, radial lines for the

JBR 21-117.R1

1
2
3 1183 two *Dbp* reporter lines are overlapping and appear as a single line. Within each organ examined, time of
4 1184 peak differed significantly in *Per2^{LucSV/+}* explants compared to *Dbp^{Luc/+}* and *Alb-Cre+ ; Dbp^{KI/+}* explants
5 1185 ($p=0.002$, Watson-Williams test). There was no significant difference in peak time between *Dbp^{Luc/+}* and
6 1186 *Alb-Cre+ ; Dbp^{KI/+}* liver tissues ($p>0.05$).
7
8
9
10
11 1187
12 1188
13
14
15
16
17
18
19
20
21
22
23
24
25
26
27
28
29
30
31
32
33
34
35
36
37
38
39
40
41
42
43
44
45
46
47
48
49
50
51
52
53
54
55
56
57
58
59
60

For Peer Review

1189

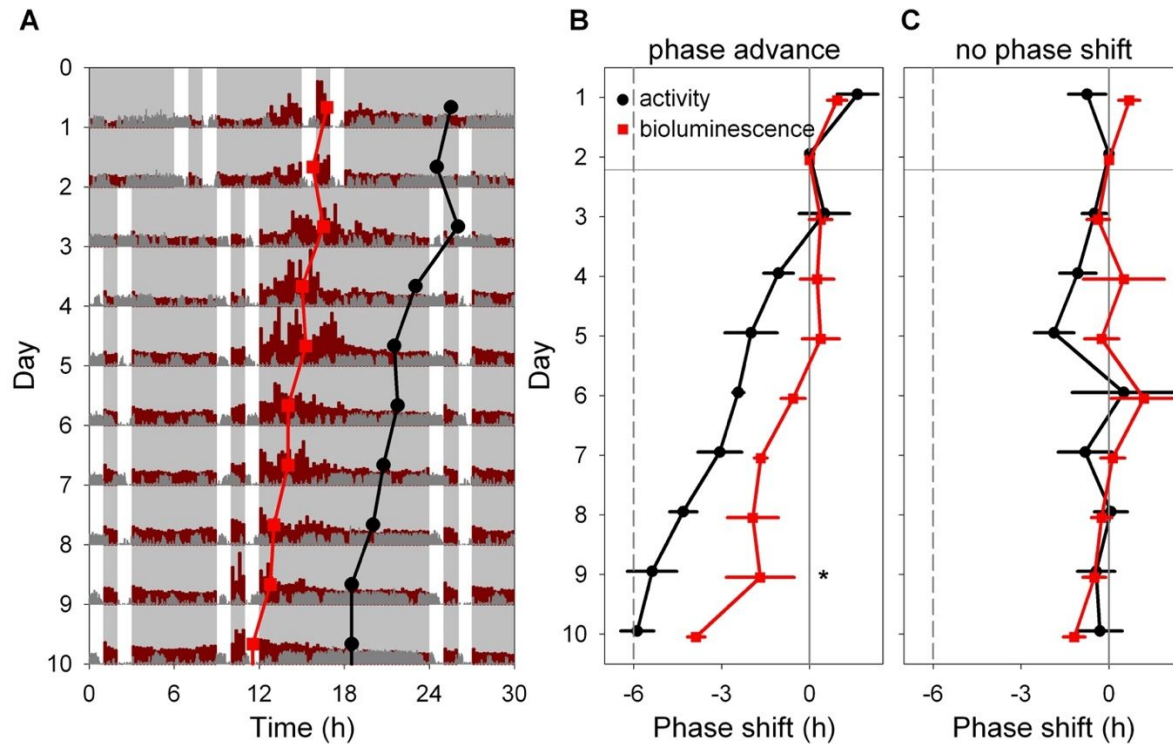


1190

1191

Figure 5. Cell-type-specific imaging of luciferase expression in SCN slices.

1
2
3 1192
4
5 1193 **A)** 24h summed bioluminescence overlaid onto bright field images of a section through the SCN from
6 1194 *Dbp^{Luc/+}* (global reporter expression, left), and in mice expressing luciferase from specific subsets of SCN
7
8 1195 neurons (NMS⁺ cells, center; AVP⁺ cells, right).
9
10 1196 **B.** Representative bioluminescence traces from single neuron-like ROIs in slices from each genotype.
11 1197 **C.** Circular plots indicate the peak time of bioluminescence rhythms from each genotype. Time is expressed
12 1198 relative to the light-dark cycle the mice were housed in prior to sacrifice; numbers >24 are used to indicate
13 1199 that these measures are recorded on the first day in culture and are plotted relative to the previous lighting
14 1200 conditions. Each slice is represented by a small dot. Placement of the dot relative to outer circle indicates
15 1201 average peak time (\pm SD), while the distance from the center corresponds to the number of cells incorporated
16 1202 in the average ($\sqrt{\text{cell\#}}$).
17
18 1203 **D-G.** Rhythm parameters by genotype. The number of slices per genotype is indicated at the base of each
19 1204 bar.
20
21 1205 **D.** Mean period (\pm SEM).
22
23 1206 **E.** Circular mean peak time (\pm SEM).
24
25 1207 **F.** Mean rhythmicity index score (\pm SEM).
26
27 1208 **G.** Mean peak time dispersal (quantified by circular SD of peak times within each slice).
28
29 1209
30
31 1210
32
33
34
35
36
37
38
39
40
41
42
43
44
45
46
47
48
49
50
51
52
53
54
55
56
57
58
59
60



1211

1212 **Figure 6. Light-induced resetting produces misalignment between rhythms in liver bioluminescence**
 1213 **and locomotor activity.**

1214 **A.** Representative double-plotted actogram showing locomotor activity (dark gray) and bioluminescence
 1215 (dark red) of an *Alb-Cre; Dbp^{KI/+}* liver reporter mouse before and after a 6-h advance of the skeleton
 1216 photoperiod consisting of four 1-h periods of light per 24-h day, as indicated by white. The skeleton
 1217 photoperiod was advanced by 6 h by shortening the dark phase after the last light pulse on Day 2. Red
 1218 squares represent the peak of the bioluminescence rhythm, while black circles represent the midpoint of
 1219 locomotor activity each day, determined by discrete wavelet transform analysis. Six hours of each cycle are
 1220 double-plotted to aid visualization. Light and dark are indicated by white and gray backgrounds,
 1221 respectively.

1222 **B.** Mean (\pm SEM) midpoint of locomotor activity (black) and peak of liver bioluminescence (red) rhythms
 1223 are shown, relative to their initial value, in a group of 4 mice exposed to a 6-h phase advance of the skeleton
 1224 photoperiod. The locomotor activity rhythm re-sets more rapidly than the bioluminescence rhythm within
 1225 animal (Significant Measure * Day interaction, and significant phase difference between the rhythms on
 1226 Day 9; Tukey HSD, $p < 0.05$).

1227 **C.** Mean (\pm SEM) time of midpoint of locomotor activity (black) and peak liver bioluminescence (red)
 1228 rhythms are shown, relative to their initial phase, in a group of 4 mice not subjected to a phase shift of the
 1229 skeleton photoperiod.

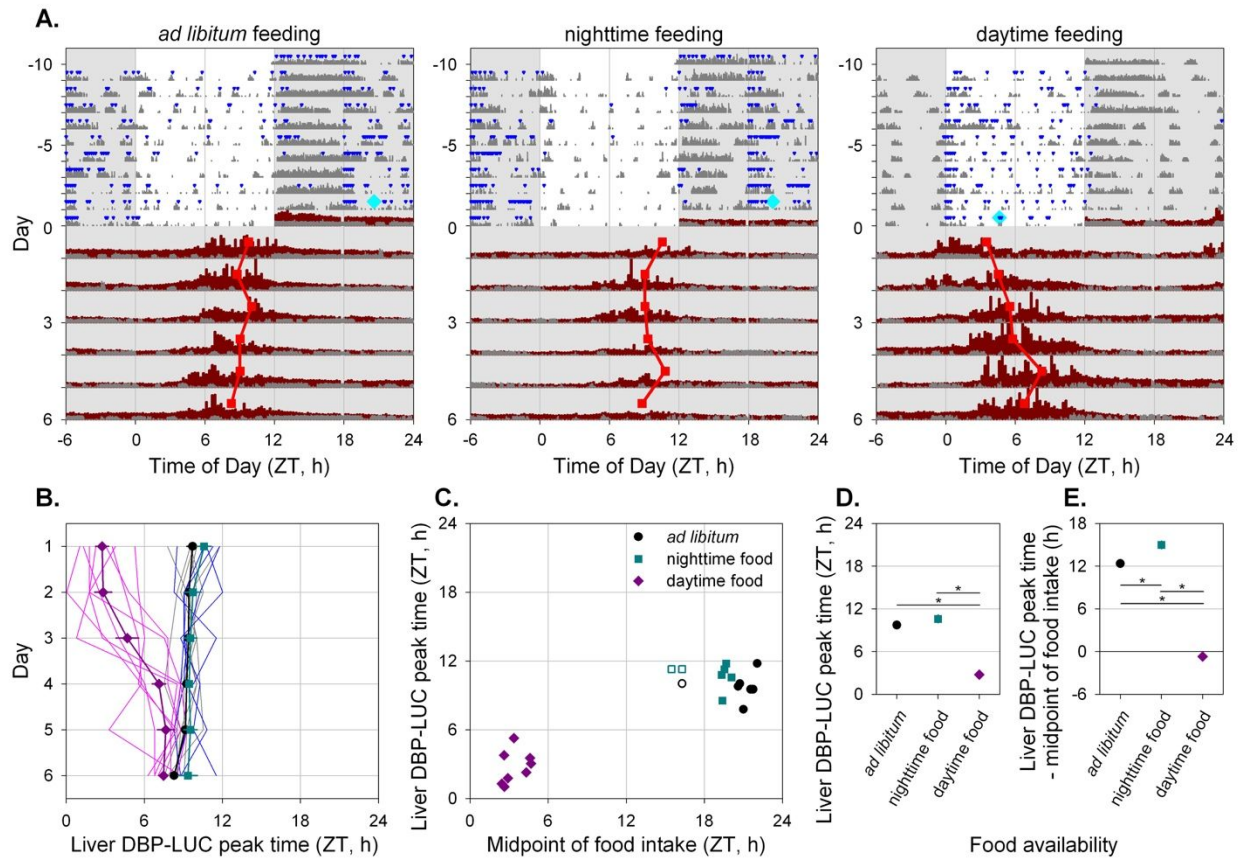


Figure 7. Time-restricted feeding alters the timing of liver bioluminescence rhythms.

- A.** Representative actograms of three *Alb-Cre; Dbp^{KI/+}* liver reporter mice exposed to the different feeding regimes as indicated above each panel. Mice were housed in 12L:12D lighting and exposed to the specified feeding regime for ten days (-10 to 0) before bioluminescence recording. Food intake (blue triangles) and general locomotor activity (dark gray) were recorded continuously. The midpoint of food intake from days -5 to 0 is indicated by a cyan diamond on day 0. Mice were transferred to the bioluminescence recording setup at the start of the dark phase and housed in constant darkness with *ad libitum* food access. Liver bioluminescence levels are depicted in dark red. Red squares represent the time of peak of the bioluminescence rhythm, determined by DWT. Six hours of each cycle are double-plotted and the y-axis has been stretched during the last 6 days to aid visualization. Light and dark are indicated by white and gray backgrounds, respectively.
- B.** Individual and mean (\pm SEM) phase of liver bioluminescence rhythms relative to clock time for three feeding groups. Mice previously exposed to *ad libitum*, nighttime and daytime feeding are plotted in grey/black, blue/cyan and magenta, respectively (key in Panel C). Prior to recording bioluminescence, mice were entrained to a 12L:12D lighting cycle with lights on at 0600. Mice

1
2
3 1247 previously exposed to daytime feeding show an advanced peak phase of liver bioluminescence that
4 1248 reverts over time in constant darkness with *ad libitum* food.
5
6 1249 C. Relationship between preceding feeding phase and peak liver bioluminescence phase for individual
7 animals on the first day under constant conditions. *Ad libitum* and night-fed groups had similar
8 1250 midpoint of food intake; three “outliers” with respect to midpoint of food intake (shown by open
9 1251 symbols) were not included in further analyses (Panels B, D and E).
10 1252
11 1253 D. Mean (\pm SEM) peak liver bioluminescence phase on the first day under constant conditions, relative
12 to clock time for the three feeding regimens. Error bars were nearly or completely contained within
13 1254 the symbols.
14 1255
15 1256 E. Mean (\pm SEM) peak liver bioluminescence phase on the first day under constant conditions, relative
16 to the midpoint of preceding food intake for the three feeding regimens. Error bars were nearly or
17 1257 completely contained within the symbols.
18 1258
19 1259
20
21
22
23
24
25
26
27
28
29
30
31
32
33
34
35
36
37
38
39
40
41
42
43
44
45
46
47
48
49
50
51
52
53
54
55
56
57
58
59
60

Table 1: Period length of locomotor activity rhythms in constant darkness, by sex and genotype

1261

1262	Genotype	Sex	N	τ_{DD} (Mean \pm SEM), h
1263	<i>Dbp</i> ^{+/+}	Male	15	23.88 \pm 0.027
1264	<i>Dbp</i> ^{KI/+}	Male	10	23.91 \pm 0.057
1265	<i>Dbp</i> ^{KI/KI}	Male	11	23.92 \pm 0.036
1266	<i>Dbp</i> ^{Luc/+}	Male	11	23.86 \pm 0.025
1267	<i>Dbp</i> ^{Luc/Luc}	Male	8	23.97 \pm 0.029
1268				
1269	<i>Dbp</i> ^{+/+}	Female	21	23.87 \pm 0.021
1270	<i>Dbp</i> ^{KI/+}	Female	9	23.89 \pm 0.036
1271	<i>Dbp</i> ^{KI/KI}	Female	11	23.79 \pm 0.030
1272	<i>Dbp</i> ^{Luc/+}	Female	8	23.82 \pm 0.053
1273	<i>Dbp</i> ^{Luc/Luc}	Female	8	23.75 \pm 0.042

1
2
3 **Supplementary Information for:**
4
5

6
7 **“Cell-type specific circadian bioluminescence rhythms in *Dbp* reporter mice”**
8
9

10
11
12 Ciarra B. Smith, Vincent van der Vinne, Eleanor McCartney, Adam C. Stowie, Tanya L. Leise,
13

14 Blanca Martin-Burgos, Penny C. Molyneux, Lauren A. Garbutt, Michael H. Brodsky,
15

16 Alec J. Davidson, Mary E. Harrington, Robert Dallmann, and David R. Weaver
17
18

19
20
21 Corresponding author: David Weaver

22 Email: David.Weaver@umassmed.edu
23
24

25
26 **This PDF file includes:**

27 Figure S1 through S7

28 Table S1
29
30
31
32
33
34
35
36
37
38
39
40
41
42
43
44
45
46
47
48
49
50
51
52
53
54
55
56
57
58
59
60

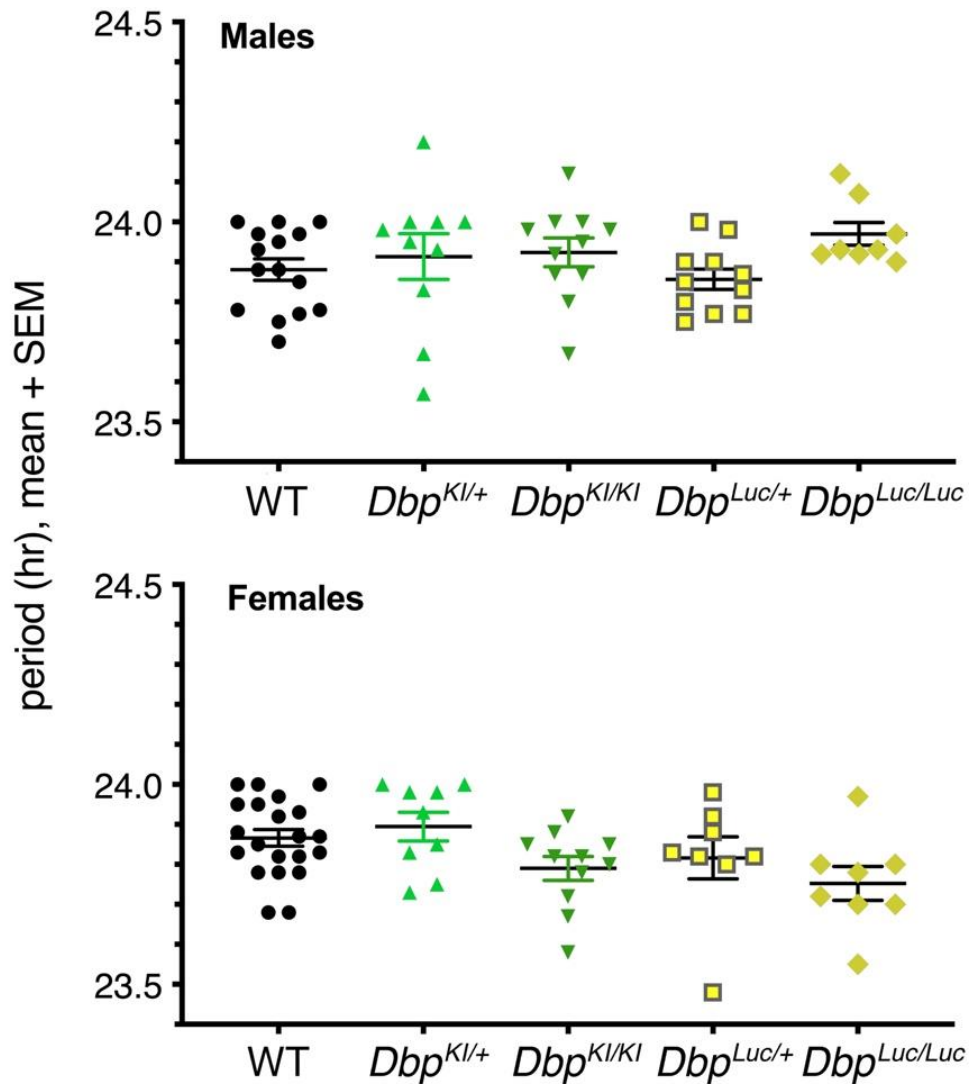


Fig. S1. Period length values of mice in constant darkness.

Values are period length values of individual mice, with mean and standard error of the mean also indicated. These data are listed in summary form (mean \pm SEM) in Table 1. See text for statistical analysis.

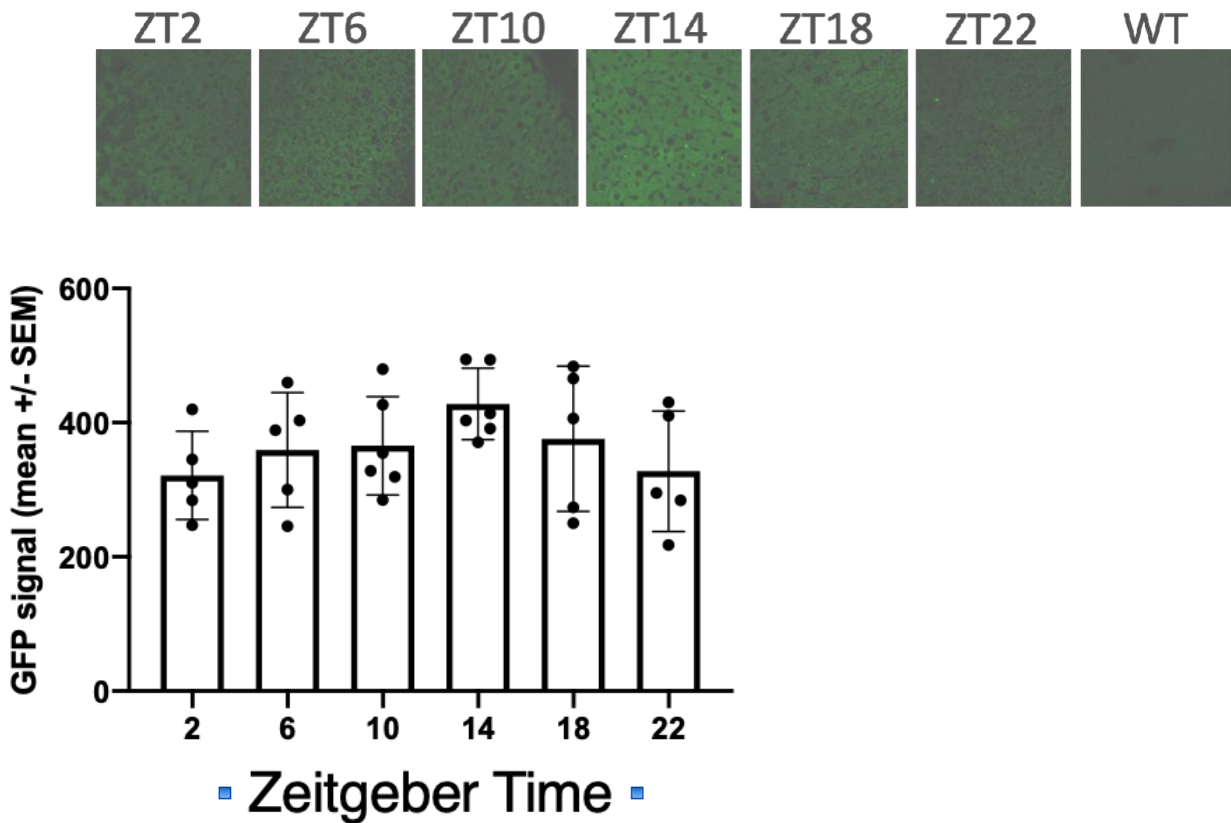


Figure S2: GFP fluorescence signal in liver sections from *Dbp^{KI/+}* mice.

Upper panels: Representative images of *Dbp^{KI/+}* liver sections at each timepoint, and in a wild-type (WT) mouse.

Lower panel: Quantification of GFP fluorescence. Each point represents mean fluorescence for the 2-4 sections from 1 mouse.

Methods: Liver tissue was collected from 5-6 *Dbp^{KI/+}* mice (n=5-6 mice per time-point) every 4 hours for 24 hours on the first day in constant darkness. To collect liver tissue, mice were anesthetized with pentobarbital and transcardially perfused with 4% paraformaldehyde and then postfixed for 8 hours. Livers were sectioned at 200 μ m using a vibratome, and sections mounted on slides with Fluoroshield with DAPI (Sigma-Aldrich). Images were captured at 40x on a Zeiss LSM 880 confocal microscope. ImageJ was used to determine mean fluorescence of 2-4 slices per animal. The average of sections from each of 3 WT mice were 41.2, 64.2 and 66.2 (mean \pm SEM = 57.18 \pm 8.02, n=3 mice).

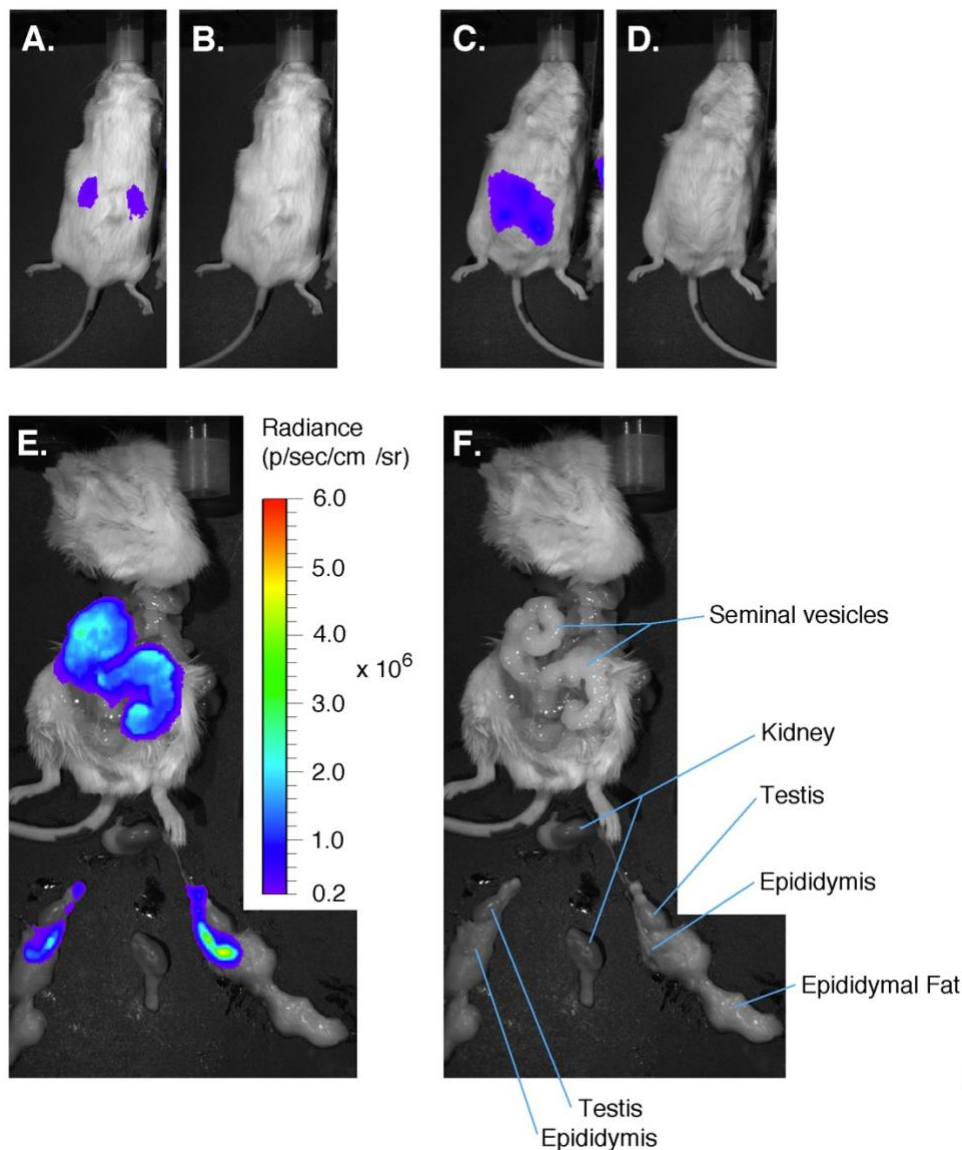


Figure S3. Bioluminescence distribution in a male 'kidney reporter' mouse.

Paired bioluminescence images (A,C,E) and photos (B,D,F) from a male albino *Ksp1.3-Cre; Dbp^{KI/+}* mouse. The radiance scale inset to Panel E applies to panels A, C, and E.

A,B: Dorsal view captured 11 minutes after injection of D-luciferin (100 μ l at 10 mM).

C,D: Ventral view captured 9 minutes after injection of D-luciferin.

E,F: Postmortem dissection identifying the main sources of bioluminescence as seminal vesicles and epididymis. The image in E was captured 14 minutes after D-luciferin injection, within 3 minute of death induced by intentional anesthetic overdose.

Representative of 9 males.

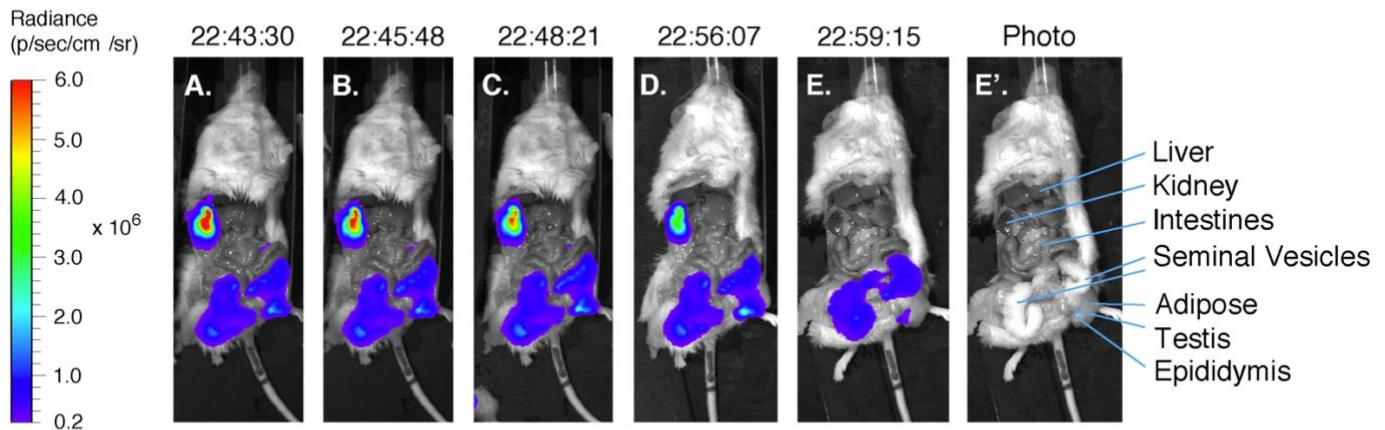


Figure S4. Postmortem change in bioluminescence distribution in a male kidney reporter.

Luciferin injection (100 μ l at 10 mM) at 22:34. The animal was anesthetized but alive in Panels A through D. Panels A-E are 9, 11, 14, 22 and 25 minutes after D-luciferin injection, respectively; clock time is shown above each panel. The radiance scale at left applies to panels A-E. E' is a photo matched to Panel E.

Note the precipitous decline in bioluminescence from the kidney and its preservation from seminal vesicles after the animal died at 22:57 from intentional anesthetic overdose. The animal's left kidney is obscured by liver and other tissues. Taken together with the external images (See Fig S3), these results indicate kidney and seminal vesicles are major sources of bioluminescence in male *Ksp1.3-Cre; Dbp^{KI/+}* mice.

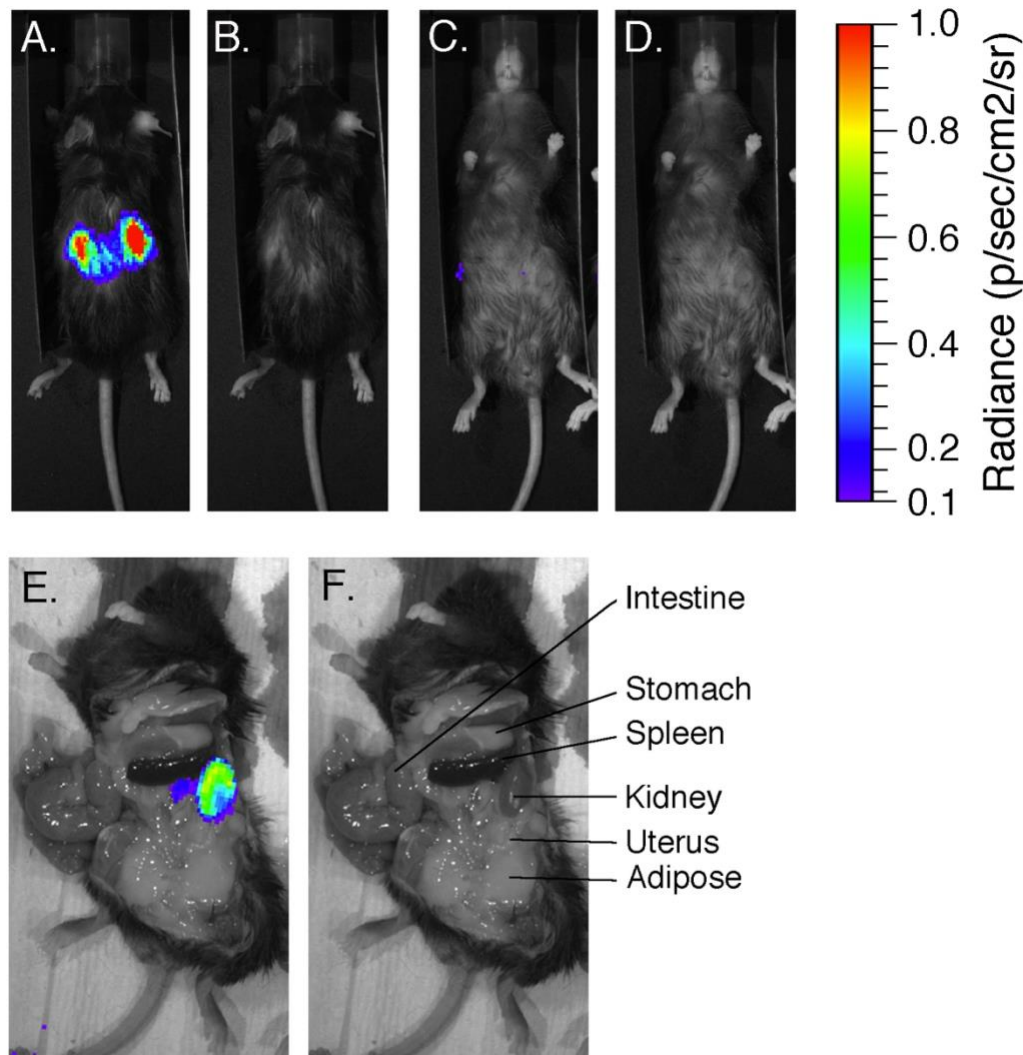


Figure S5. Bioluminescence originates from the kidney in female ‘kidney reporter’ mice.

A-D Matched bioluminescence images and photos of intact mice.

A,B: Dorsal view captured 9 minutes after D-luciferin injection (100 ul at 10 mM).

C,D: Ventral view captured 10.5 minutes after D-luciferin injection.

E,F: Postmortem dissection identifies the source of bioluminescence as the kidney. The image was captured 15 minutes after D-luciferin injection, within 3 minute of death induced by intentional anesthetic overdose. The animal’s right kidney is obscured by other abdominal contents. External views representative of 16 females. Dissection representative of 7 females.

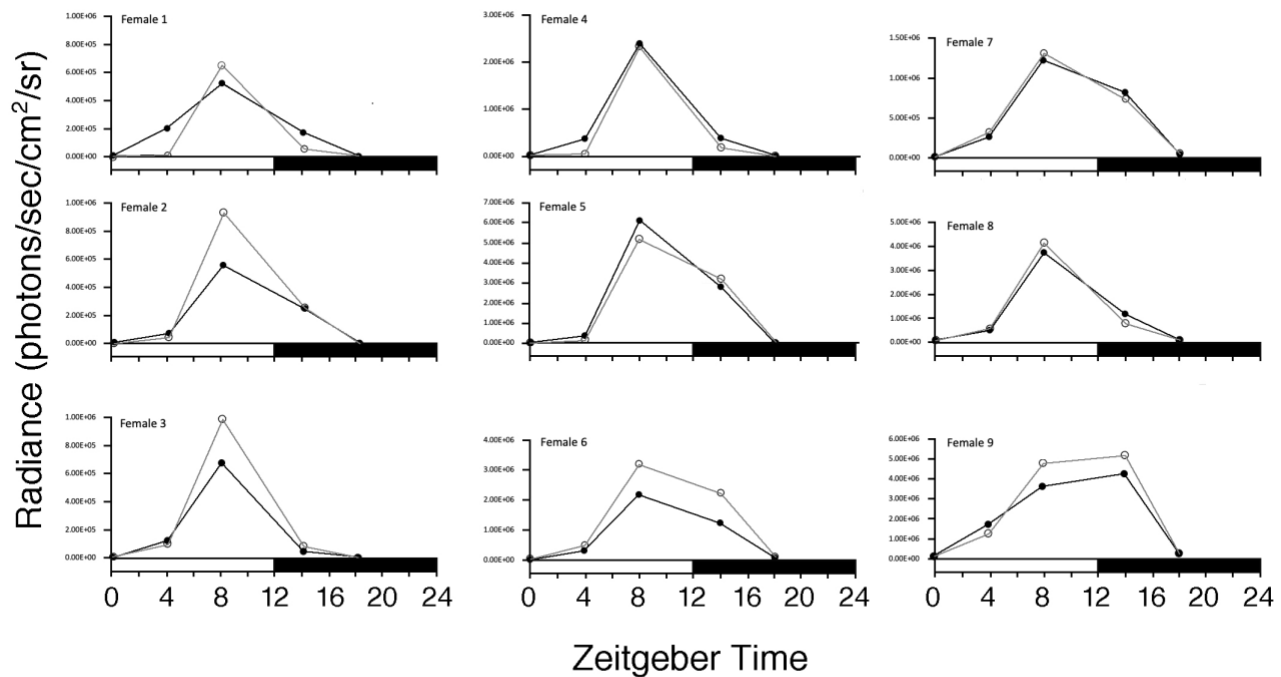


Figure S6: Bioluminescence rhythms in female kidney reporter mice.

Quantitative assessment of renal bioluminescence rhythms in intact female kidney reporter mice (albino *Ksp1.3-Cre; Dbp^{KI/+}*, n=9). For each female, right kidney (filled symbols, black line) and left kidney (open symbols, gray line) values are shown. Images (dorsal view) were captured 9 to 9.5 min after injection of D-luciferin (100 μ l at 10 mM). Time-points are ZT0-1, 4-5, 8-9, 14-15, and 18-19; data are plotted at the beginning of each interval. In 8 of 9 mice, the highest level of bioluminescence occurred at ZT8. Friedman one-way analysis of variance indicated a significant difference among the timepoints ($F_T = 32.71$, $k=5$, $n=9$, $p < 0.0001$). Dunn's test revealed that the ranks at the ZT8 timepoint differed significantly from the ranks at ZT0 and ZT18 (multiplicity-corrected, two-tailed p -value < 0.0005), with a trend toward a difference at ZT4 (multiplicity-corrected, two-tailed p -value = 0.0684). Ranks at ZT8 and ZT14 did not differ significantly.

Methods: Radiance was assessed using Living Image software for ROI's of fixed size for each kidney at the five Zeitgeber time-points. For each kidney, the rank order of bioluminescence levels among the five timepoints was determined. When the order was not identical for both kidneys within an animal (as occurred twice), the bioluminescence values from the two kidneys at each time-point were averaged; the ranking of timepoints was then determined using the average values. Thus, bioluminescence from both kidneys was considered, but each animal contributed only one set of rankings for statistical analysis.

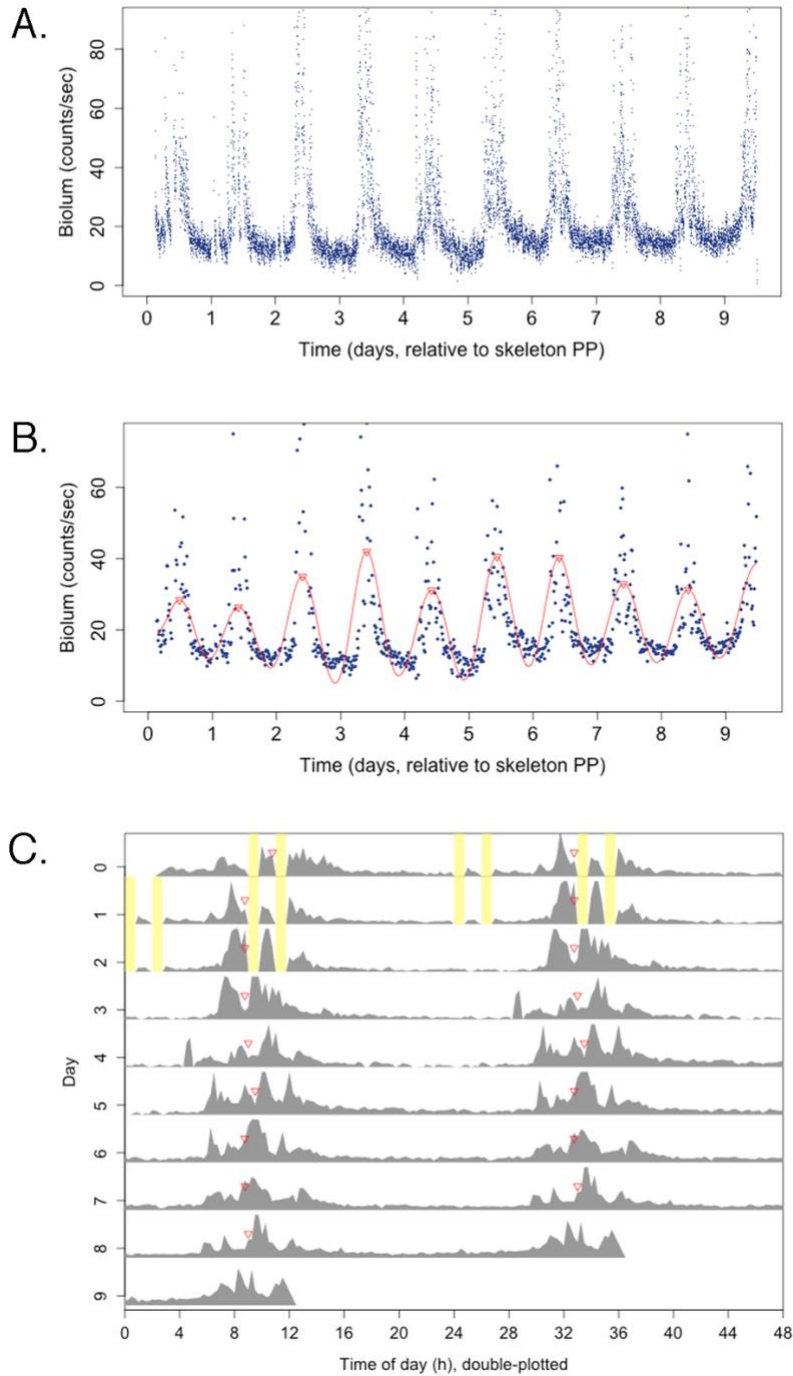


Figure S7. Bioluminescence Rhythms from a Liver Reporter Mouse. Panels A,B and C represent the same data, from a female mouse with 2 mM D-luciferin in its drinking water. Panel A shows raw bioluminescence data, excluding outliers above the 98th percentile. Panel B shows 15-minute median binned values as blue dots, the DWT circadian component plus smooth as a red curve, and the DWT-calculated time of peak as red triangles. Panel C displays the bioluminescence data (gray) in actogram format, with the skeleton photoperiod in yellow and red triangles marking time of peak for each day. Time zero is set to the start of the first dawn light pulse of the skeleton photoperiod (skeleton PP) during bioluminescence recording.

Table S1. PCR Primer Pairs.**1. Primer Pairs for Confirming the Targeted *Dbp* Locus**Primer pair C (Internal to the construct; forward in GFP, reverse in Luc2)*Dbp*-C- Forward 5' - CAAGGTGAACTTCAAGATCCGC -3'*Dbp*-C-Reverse 5' - CCCATGCTGTTTCAGCAGCTCG -3'Primer pair F (spans 5' end; forward in intron 3 outside construct, reverse in T2A sequence)*Dbp*-F- Forward 5' - GGAAGCATCTTTTCCAGCTGG - 3'*Dbp*-F-Reverse 5' - TTCCTCTGCCCTCTCCACTGC - 3'Primer Pair H (spans 3' end; forward in Luciferase, reverse in 3' UTR outside construct)*Dbp*-H- Forward 5' - GATTCTCATTAAGGCCAAGAAGG - 3'*Dbp*-H- Reverse 5' - CATGGCGAGTTGGTGGAACCAGC - 3'Primer Pair 'confirm' (external to and spanning the entire construct)

(forward in intron 3 outside the construct, reverse in 3' UTR outside the construct)

Dbp-span-Forward 5' - GATGTGTCCTAACAAGCTGGAGC - 3'*Dbp*-span-Reverse 5' - AAGCCACAAGCCTGAACGAGC - 3'**2. Genotyping Primer sets***Dbp* Primer set "4A" (Common forward primer in exon 4, allele-specific reverse primers)*Dbp*-4A-Forward 5' - TGCTGTGCTTTTACGCTACCAGG - 3'*Dbp*-4A-Reverse in GFP 5' - AGTCGTGCTGCTTCATGTGGTCG - 3'*Dbp*-4A-Reverse in Luc2 5' - TCGTTGTAGATGTCGTTAGCTGG - 3'*Dbp*-4A-Reverse in 3'UTR 5' - TTCAGGATTGTGTTGATGGAGGC - 3'Primer set *Clock/Cre* {*Clock* J (internal control) plus *Cre*-370, used as a 4-primer mix}*Clock* Forward 5'- GCAAGAAGAATAAGGAAAATTCAA-GAGCAACTTCAGATGGTCCATGGTCAA-GGGCTACAGTT - 3'*Clock* Reverse 5'- TAGTGCCCTAGATGGCCCTGTTGG -3'*Cre*-370 Forward 5' - ACCTGAAGATGTTTCGCGATTATCT - 3'*Cre*-370 Reverse 5' - ACCGTCAGTACGTGAGATATCTT - 3'*Per2*::LUCIFERASE(SV) (Common forward primer, allele-specific reverse primers)*Per2* Common Forward 5' - CTGCGAGAGTGAGGAGAAAGGC - 3'*Per2* WT-specific Reverse 5' - GGATTTCTCCTAAACCTCCC - 3'*Per2* Luc-specific Reverse 5' - GTAGATGAGATGTGACGAACG - 3'

3. Primer pairs for Generating DIG-labeled Probes

1
2
3
4
5
6 *Actin* Forward: 5' - TCAGAAGGACTCCTATGTGGG - 3'
7 *Actin* Reverse: 5' - GATCCACACAGAGTACTTGCG - 3'
8
9 *Dbp* Forward: 5' - AATGACCTTTGAACCTGATCCC - 3'
10 *Dbp* Reverse: 5' - TCACAGTGTCCCATGCTGGG - 3'
11
12 *GFP* Forward: 5' - CTGAAGTTCATCTGCACCACCG - 3'
13 *GFP* Reverse: 5' - GTGCTCAGGTAGTGGTTGTCGG - 3'
14
15
16 *Luc2* Forward: 5' - GCTTCGAGGAGGAGCTATTCTTGC - 3'
17 *Luc2* Reverse: 5' - CAGCAGGATGCTCTCCAGTTCGG - 3'
18
19
20
21
22
23
24
25
26
27
28
29
30
31
32
33
34
35
36
37
38
39
40
41
42
43
44
45
46
47
48
49
50
51
52
53
54
55
56
57
58
59
60

For Peer Review